Molecular Therapy
Nucleic Acids
Original Article

Specific *DMPK*-promoter targeting by CRISPRi reverses myotonic dystrophy type 1-associated defects in patient muscle cells

Florent Porquet,[1,2,3] Lin Weidong,[1] Kévin Jehasse,[2] Hélène Gazon,[1] Maria Kondili,[3] Silvia Blacher,[5] Laurent Massotte,[2] Emmanuel Di Valentin,[4] Denis Furling,[3] Nicolas Albert Gillet,[6] Arnaud François Klein,[3,7] Vincent Seutin,[2,7] and Luc Willems[1,7]

[1]Laboratory of Molecular and Cellular Epigenetics, GIGA-Cancer, ULiège, 4000 Liège, Belgium; [2]Laboratory of Neurophysiology, GIGA-Neurosciences, ULiège, 4000 Liège, Belgium; [3]Sorbonne Université, INSERM, Institut de Myologie, Centre de Recherche en Myologie, 75013 Paris, France; [4]Viral Vector Platform, GIGA, ULiège, 4000 Liège, Belgium; [5]Laboratory of Biology of Tumor and Development, GIGA-Cancer, ULiège, 4000 Liège, Belgium; [6]Namur Research Institute for Life Sciences (NARILIS), Integrated Veterinary Research Unit (URVI), University of Namur, 5000 Namur, Belgium

Myotonic dystrophy type 1 (DM1) is a neuromuscular disease that originates from an expansion of CTG microsatellites in the 3′ untranslated region of the *DMPK* gene, thus leading to the expression of transcripts containing expanded CUG repeats (*CUGexp*). The pathophysiology is explained by a toxic RNA gain of function where *CUGexp* RNAs form nuclear aggregates that sequester and alter the function of MBNL splicing factors, triggering splicing misregulation linked to the DM1 symptoms. There is currently no cure for DM1, and most therapeutic strategies aim at eliminating *CUGexp-DMPK* transcripts. Here, we investigate a *DMPK*-promoter silencing strategy using CRISPR interference as a new alternative approach. Different sgRNAs targeting the *DMPK* promoter are evaluated in DM1 patient muscle cells. The most effective guides allowed us to reduce the level of *DMPK* transcripts and *CUGexp*-RNA aggregates up to 80%. The *CUGexp-DMPK* repression corrects the overall transcriptome, including spliceopathy, and reverses a physiological parameter in DM1 muscle cells. Its action is specific and restricted to the *DMPK* gene, as confirmed by genome-wide expression analysis. Altogether, our findings highlight *DMPK*-promoter silencing by CRISPRi as a promising therapeutic approach for DM1.

INTRODUCTION

Myotonic dystrophy type 1 (DM1) is a multisystemic pathology characterized by a large neuromuscular component. Indeed, the patients develop myotonia, progressive muscular weakness, atrophy, and cardiac arrhythmias, as well as hypersomnia, mood disorders, and cognitive impairments, due to central nervous system (CNS) defects. Muscular and cardiac manifestations lead to a reduced lifespan and induce, among the other symptoms, acute disabilities, both neuropsychological/cognitive and physical.[1,2] DM1 is the most prevalent muscular dystrophy in adults, with an estimated worldwide prevalence of 1/8,000. Locally, DM1 can reach even higher prevalence, 1/2,100 in the state of New York (USA) or 1/530 in the region of Saguenay-Lac St-Jean (Canada).[3,4] Overall, the development of therapies for DM1 patients represents an important unmet medical need.

DM1 is an autosomal dominant genetic disease caused by the amplification of CTG microsatellites (>50 repeats) within the 3′ untranslated region (UTR) of the DM1 protein kinase (*DMPK*) gene.[5] The expansions reach up to several thousand CTG repeats and, globally, their length correlates with the severity of symptoms and earlier age of onset.[6] The pathophysiology of DM1 is explained by a toxic RNA gain-of-function mechanism linked to the expression of the *CTG*-expanded *DMPK* allele, resulting in transcripts with a pathological expansion of CUG triplets (*CUGexp*).[7] *CUGexp-DMPK* mRNAs are retained in the nucleus as discrete aggregates, also called foci,[8,9] and sequester Muscleblind-like (MBNL) RNA binding proteins that have binding affinity for YGCY consensus sites.[10] The resulting loss of functional MBNL is considered to play a major role in DM1 pathophysiology,[11] a hypothesis corroborated by transgenic mice deficient for MBNL protein, which recapitulate DM1-like phenotypes.[12–15] Due to its regulatory action on RNA metabolism, impaired MBNL activity alters the transcriptome of DM1 cells, notably through alternative splicing misregulation that contributes to the clinical symptoms of DM1 patients.[16] In particular, abnormal splicing of *CLCN1*, *INSR*, *BIN1*, *DMD*, and *SCN5A* pre-mRNAs has been associated with myotonia, insulin resistance, muscle weakness, dystrophic process, and cardiac conduction

Received 26 August 2022; accepted 10 May 2023;
https://doi.org/10.1016/j.omtn.2023.05.007.

[7]These authors contributed equally

Correspondence: F. Porquet, Laboratory of Molecular and Cellular Epigenetics, GIGA-Cancer, ULiège, 4000 Liège, Belgium.
E-mail: f.porquet@institut-myologie.org
Correspondence: A.F. Klein, Sorbonne Université, INSERM, Institut de Myologie, Centre de Recherche en Myologie, 75013 Paris, France.
E-mail: a.klein@institut-myologie.org

defects, respectively.[17–23] In summary, while the functional loss of MBNL is a major mechanism leading to DM1 symptoms, the expression of mutant *CUGexp-DMPK* transcripts remains the primary and necessary trigger of DM1.

Currently, only symptomatic care is offered to DM1 patients,[24] but several strategies are under development to provide a therapy to patients. To maximize the expected clinical benefit, most of the therapeutic approaches aim at targeting the toxic *CUGexp-DMPK* transcript to either degrade and reduce its level or prevent the deleterious sequestration of MBNLs.[25] The breakthrough clustered regularly interspaced short palindromic repeats/CRISPR-associated protein 9 (CRISPR-Cas9) technology has also opened up promising avenues in DM1 to either remove the pathogenic CTG expansion from the *DMPK* mutant allele by genome editing[26] or slow down *DMPK* transcription by targeting the CTG tract with a nuclease-free derivative.[27] The toxic *CUGexp-DMPK* transcript can even be directly degraded by RNA-targeting Cas9 directed to the CUG repeats.[28]

To develop an alternative approach that combines both specificity and effectivity, we propose to inhibit the expression of the toxic *CUGexp-DMPK* transcripts by specifically targeting the *DMPK* promoter using the CRISPR interference system (CRISPRi). CRISPRi is derived from the CRISPR-Cas9 system and allows us to specifically reduce the expression of a targeted gene.[29,30] It is composed of a single guide RNA (sgRNA) associated with a dead Cas9 (dCas9), a protein devoid of endonuclease activity, and fused to the human Krüppel-associated box (KRAB) transcription inhibitory domain.[31] While steric hindrance by the dCas9 participates in inhibition of the target gene,[32] the KRAB domain induces repressive epigenetic modifications at the targeted loci,[29,33,34] including in human muscle cell models.[35]

To repress *DMPK* expression, we designed sgRNAs targeting the *DMPK* promoter and evaluated the CRISPRi strategy in immortalized muscle cells derived from a DM1 patient. We showed that this approach represses the expression of *CUGexp-DMPK* transcripts, resulting in the correction of DM1-specific molecular and cellular hallmarks, and, most importantly, is combined with transcriptomic specificity. Our proof-of-concept study highlights this *DMPK*-promoter-silencing approach as a novel promising therapeutic strategy for DM1.

RESULTS

Screening of CRISPRi constructs targeting the *DMPK* promoter in differentiated DM1 patient muscle cells

To establish our *DMPK*-promoter targeting strategy by CRISPRi, we designed 13 sgRNAs (sgDMPK; Figure 1A and Table 1) *in silico* within the promoter region of the human *DMPK* gene in the immediate vicinity of the transcription start site (TSS; chr19 [GRCh37/hg19]:46.285.815) in addition to three sgRNAs that do not target the human genome (sgNT; Table 1). Each sgRNA was cloned in an all-in-one lentiviral construct containing the dCas9-KRAB sequence (Figure S1B). Lentiviral vectors were then used to transduce immortalized DM1 patient-derived myoblasts (myoDM1) expressing a mutant *DMPK* allele with more than 2,600 CTG repeats. Stable cell lines expressing both dCas9/KRAB protein and one sgRNA (sgDMPK or sgNT) were generated (Figure S1A). Subsequently, myoblasts were differentiated into myotubes, to initiate the physiological induction of *DMPK* expression by differentiation of skeletal muscle cells.[36–38]

To assess the efficacy of the CRISPRi constructs, we performed a primary screen based on the quantification of nuclear *CUGexp-DMPK* RNA foci as a direct marker of *CUGexp-DMPK* expression. Fluorescence *in situ* hybridization (FISH) analysis with a Cy3-labeled $(CAG)_5$ probe was used to detect *CUGexp-DMPK* RNA foci and revealed foci accumulation in almost all nuclei of differentiated myoDM1 cells treated with sgNT (Figure 1B, top). In contrast, a reduction in nuclear focus number and intensity was observed in myoDM1 cells treated with sgDMPKs, as shown for sgDMPK_2 (Figure 1B, bottom). To quantify these changes, the density of nuclear foci, defined as the ratio of the total area occupied by the nuclear foci over the total nuclear area, was measured (Figure 1C). This analysis showed a significant reduction in density of the foci following the expression of 9 of the 13 sgDMPKs compared with all sgNTs. In particular, sgDMPK_2-treated cells showed the lowest density, representing a reduction of 80%. This condition was closely followed by a group of sgDMPKs (sgDMPK_3, _4, _5, _11, and _12) that yielded a similar decrease of 70%, whereas the remaining sgDMPKs were less (<50% of inhibition) or not effective (Figure 1C).

Given their efficacy at decreasing the level of the *CUGexp*-foci, sgDMPK_2, as the most effective guide, as well as sgDMPK_5 and sgDMPK_12, according to their proximity to the TSS of the *DMPK* gene,[30] were selected for further assessments.

Validation of *DMPK*-promoter silencing approach by CRISPRi in DM1 muscle cells

To validate this *DMPK*-promoter silencing strategy, we supported the reduction of the level of *DMPK* transcripts by qRT-PCR analysis for the three selected guides, sgDMPK_2, sgDMPK_5, and sgDMPK_12. Differentiated myoDM1 cells expressing sgRNAs targeting the *DMPK* promoter showed a significant diminution of *DMPK* transcript levels relative to sgNT-expressing cells, reflecting an inhibition of 80% for *DMPK* expression (Figure 2A). The same effect on *DMPK* expression was also confirmed in differentiated non-DM1 muscle cells (myoWT derived from an unaffected donor) expressing the selected CRISPRi constructs (Figure S1C). Similar results in both wild-type (WT) and DM1 cells were corroborated by normalizing *DMPK* gene expression to either *TBP* or *RPL0* as a reference gene (Figures S1D–S1G).

As the level of the *CUGexp-DMPK* transcripts is reduced by the *DMPK*-silencing approach in FISH and qRT-PCR assays, we examined the nuclear localization of the MBNL1 protein by combined

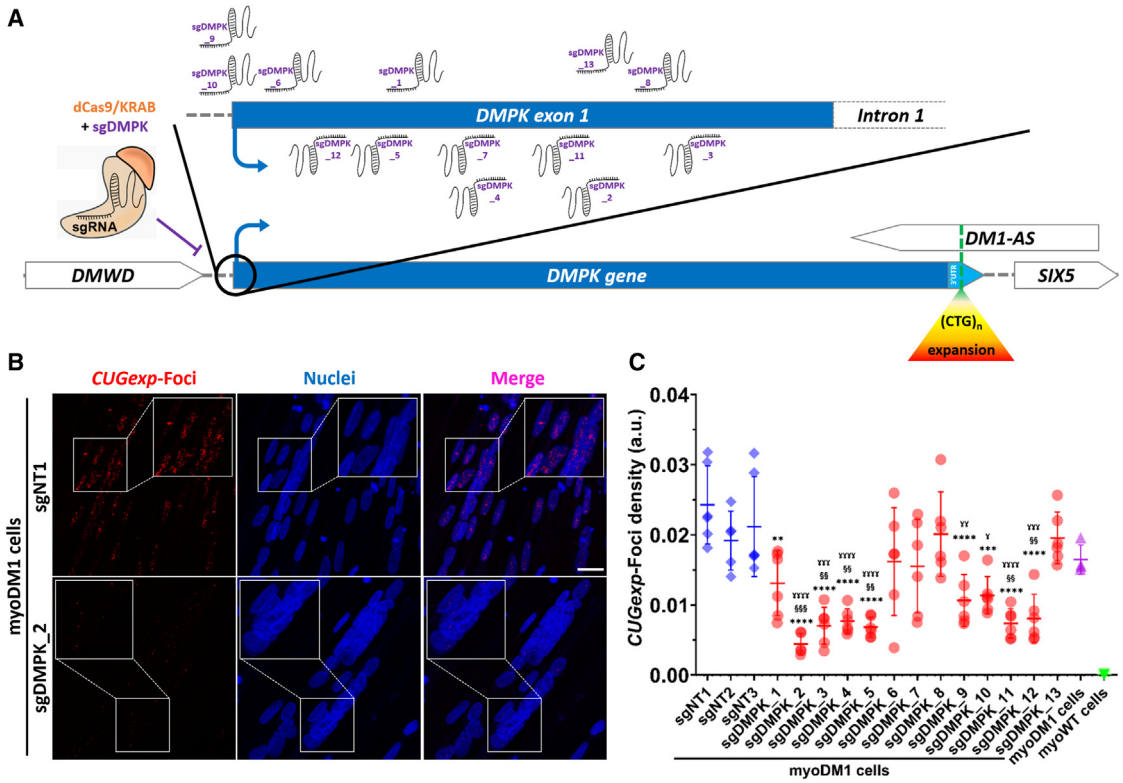

Figure 1. Screening of sgRNAs targeting the *DMPK* promoter region based on *CUGexp* foci in differentiated DM1 patient-derived muscle cells

(A) Relative genomic localization of the 13 sgRNAs targeting the *DMPK* promoter region (sgDMPK) with the CRISPRi system at the human *DMPK* locus (blue boxes) located between the *DMWD* and the *SIX5* loci (white boxes). The pathogenic trinucleotide repeat expansion $(CTG)_n$ is localized at the terminal exon of the *DMPK* gene. This expansion is also included in the antisense *DMPK* transcript (*DM1-AS*, upper white box). (B) Representative microscopic observations of the nuclear *CUGexp* foci from DM1 myotubes treated by the control guide, sgNT1, or a guide targeting the *DMPK* promoter, sgDMPK_2. The *CUGexp* foci were labeled by FISH with a 5′-Cy3-$(CAG)_5$-3′ probe (in red), while the nuclei were stained by DAPI (in blue). Image acquisition was done using a Zeiss LSM880 confocal AiryScan at 40× original magnification with 12 stacks followed by a maximal projection. Scale bar, 25 μm. (C) Automated quantification of nuclear *CUGexp* foci density in DM1 myotubes (myoDM1) treated by non-target guides (sgNT1 to 3) compared with guides targeting the *DMPK* promoter (sgDMPK_1 to _13). The values of non-treated DM1 or WT (myoWT) cells are also displayed as references. The focus density is defined by the overall area occupied by nuclear foci divided by total DAPI area. Statistics: one-way ANOVA followed by *post hoc* Tukey tests. **post hoc* test versus sgNT1, ^{Y}*post hoc* test versus sgNT2, $^{Y}p < 0.05$; **,^{YY},$^{\S\S}p < 0.01$; ***,^{YYY},$^{\S\S\S}p < 0.001$; ****,$^{YYYY}p < 0.0001$. Data are shown as the mean ± SD, n = 6 replicate transductions; >500 nuclei per n.

FISH and immunofluorescence. While MBNL1 is mainly colocalized with nuclear *CUGexp* foci in differentiated myoDM1 cells expressing sgNT1 (Figure 2B, top), it relocalizes throughout the nucleoplasm in differentiated myoDM1 cells expressing sgDMPK_2, along with the reduction of the *CUGexp* foci (Figure 2B, bottom).

To confirm the recovery of MBNL1 activity in treated DM1 muscle cells, alternative splicing events regulated by MBNL1, such as *DMD* exon 78, *BIN1* exon 11, and *LDB3* exon 11, were measured via percentage splice in (PSI) index by RT-PCR.[39–42] Overall, the treatment with sgDMPKs resulted in the significant correction of *BIN1*, *DMD*, and *LDB3* splicing in DM1 cells (Figures 2C–2E), up to 61%, 50%, and 56%, respectively. Among the selected guides targeting the *DMPK* gene, sgDMPK_2 exhibited a significantly higher improvement for *DMD* and *LDB3* defects compared with sgDMPK_12 (Figures 2D and 2E), consistent with the trend of elevated efficacy of this sgRNA to eliminate RNA foci, as shown by FISH. Since the state of muscular differentiation could also have an impact on alternative splicing,[43] we showed that the *DMPK* silencing by CRISPRi leads also to the correction of splicing defects, which are independent of the state of differentiation (A.F.K. et al., unpublished data) and used as efficacy markers to evaluate other therapeutic approaches,[39,40] including the previous *DMD* exon 78 (Figure 2D) as well as *MBNL1* exon 5 and *SORBS1* exon 25 (Figure S2).

Finally, the reduction in *DMPK* level was also observed to be of similar efficacy in primary cells derived from a DM1 patient or a healthy individual (Figures S3A and S3B). The *DMPK*-promoter targeting is also associated with corrections of the DM1 hallmarks in the primary DM1 cells (Figures S3C–S3F).

Therefore, the *DMPK*-promoter inhibitory strategy by CRISPRi leads to a robust correction of DM1 hallmarks in muscle cells derived from a DM1 patient.

Table 1. Features of sgRNAs used to silence the *DMPK* gene, sgDMPKs, and the non-target guides, sgNTs

Designation	Sequence	PAM sequence	Orientation	Distance from TSS relative to 3′ sgRNA	Localization (GRCh37/hg19)
sgDMPK_1	5′-GACAGGCAGACATGCAGCCA-3′	5′-GGG-3′	antisense	+111 bp	chr19:46.285.702–46.285.724
sgDMPK_2	5′-GAGCCGCCTCAGCCGCACCT-3′	5′-CGG-3′	sense	+215 bp	chr19:46.285.581–46.285.603
sgDMPK_3	5′-GCCCAGGAGAAGGTCGAGCA-3′	5′-GGG-3′	sense	+278 bp	chr19:46.285.518–46.285.540
sgDMPK_4	5′-GCTCGGGGTCCTCCTGTCAC-3′	5′-AGG-3′	sense	+146 bp	chr19:46.285.650–46.285.672
sgDMPK_5	5′-GCTGCATGTCTGCCTGTCCC-3′	5′-TGG-3′	sense	+89 bp	chr19:46.285.707–46.285.729
sgDMPK_6	5′-GGGAGAAGGGGAGGAGGCCT-3′	5′-CGG-3′	antisense	+42 bp	chr19:46.285.771–46.285.793
sgDMPK_7	5′-GGTCCTCCTGTCACAGGGCC-3′	5′-TGG-3′	sense	+140 bp	chr19:46.285.656–46.285.678
sgDMPK_8	5′-GGTGTTGGACCCGGGCTTCC-3′	5′-TGG-3′	antisense	+263 bp	chr19:46.285.550–46.285.572
sgDMPK_9	5′-GGTTAAGGCTGGGAGGCGGG-3′	5′-AGG-3′	antisense	−1 bp	chr19:46.285.813–46.285.835
sgDMPK_10	5′-GTTAAGGCTGGGAGGCGGGA-3′	5′-GGG-3′	antisense	0 bp	chr19:46.285.812–46.285.834
sgDMPK_11	5′-CCTCGGCTGACATGTTGGAC-3′	5′-AGG-3′	sense	+198 bp	chr19:46.285.598–46.285.620
sgDMPK_12	5′-TCTCTGGCCACTTCTCTCTG-3′	5′-CGG-3′	sense	+52 bp	chr19:46.285.744–46.285.766
sgDMPK_13	5′-TGTCAGCCGAGGTGCGGCTG-3′	5′-AGG-3′	antisense	+226 bp	chr19:46.285.587–46.285.609
sgNT1	5′-CGCGATAGCGCGAATATAT-3′				
sgNT2	5′-TTATATCCAACACTTCGTG-3′	N/A	N/A	N/A	N/A
sgNT3	5′-GCACTACCAGAGCTAACTCA-3′				

Transcriptomic transition of DM1 cells toward normal pattern by *DMPK*-silencing strategy in DM1 cells

To assess the overall effect of the most efficient *DMPK*-repressing guide, sgDMPK_2, on both alternative splicing and gene expression in DM1 muscle cells, we performed a deep paired-end RNA sequencing (>2 × 80M reads/sample, four independent replicates).

This analysis unveiled 2,432 unique splicing events (false discovery rate [FDR] ≤ 0.05; ΔPSI ≥ |0.15|; Table S1) for DM1 cells, representing a distinctive splicing pattern compared with the WT condition, while the *DMPK*-promoter silencing by sgDMPK_2 induced a substantial transition of treated DM1 cells toward the WT profile (Figure 3A). This transition reflected a correction of spliceopathy by the *DMPK*-silencing approach, with a large proportion (79%) of improved splice events (≥10% correction) in treated DM1 cells (Figure 3B). Among these splicing corrections, *BIN1* exon 11, *DMD* exon 78, and *LDB3* exon 11 have similar ranges of correction (50.5%, 42.6%, and 63.3%, respectively) compared with RT-PCR analysis, validating the RNA sequencing.

Gene expression analysis revealed, in addition, that 1,913 genes are differentially expressed in DM1 muscles cells compared with WT cells (FDR ≤ 0.05; log2 fold change [FC] ≥ |1|; Figure 3C and Table S1). The *DMPK* inhibition by sgDMPK_2 in DM1 cells also led to a transition toward the WT profile. Nearly 75% of deregulated gene expression in DM1 was involved in this transition (≥10% correction; Figure 3D).

Among the replicates where the *DMPK* gene is targeted, the fourth (N_4) displayed a lower improvement, as observed for both gene expression and alternative splicing (Figures 3A and 3C). Whereas the expression of the *DMPK* gene and dCas9 transgene (Figures S4A and S4B) did not support this variation, the lower level of differentiation of this replicate, measured using markers such as Myogenin (*MyoG*) and *Myosin Heavy Chain 3* (*MyH3*) gene expression (Figures S4C and S4D),[44] could explain the difference, given the potential impact of the level of cellular differentiation on the transcriptome.[43]

In summary, *DMPK* repression by CRISPRi allows us to restore to a large extent the normal transcriptomic profile of DM1 muscle cells for both gene expression and alternative splicing.

Reversal of a physiological defect through the *DMPK*-repressing approach in DM1 cells

Gene ontology (GO) term enrichment analysis of these 1,913 gene expression changes (FDR ≤ 0.05; log2 FC ≥ |1|) showed that disturbed gene expression in DM1 muscle cells is related to structural functions, cell signaling, and cellular ionic currents (Figure 4A). Interestingly, the expression of genes that are linked to the cellular ionic currents GO terms was improved by at least 75% following *DMPK* inhibition in DM1 muscle cells (red arrows, Figure 4A), suggesting a potential physiological impact of this group of genes on treated cells.

To test this hypothesis, we performed a whole-cell patch clamp in WT, DM1, and treated DM1 muscle cells to record the electrical membrane resistance (Rm). This electrophysiological parameter reflects the overall dynamics of ionic membrane currents in cells.[45] First, we confirmed that the Rm of myoWT cells was lower than that of the myoDM1 cells (Figures 4B and 4C), indicating altered cellular ionic currents in disease cells. Next, we measured this parameter in myoDM1 treated with sgDMPK_2 and found that the *DMPK*-silencing guide decreased the Rm of myoDM1 cells to levels similar to those measured in myoWT cells (Figures 4B and 4C). This analysis

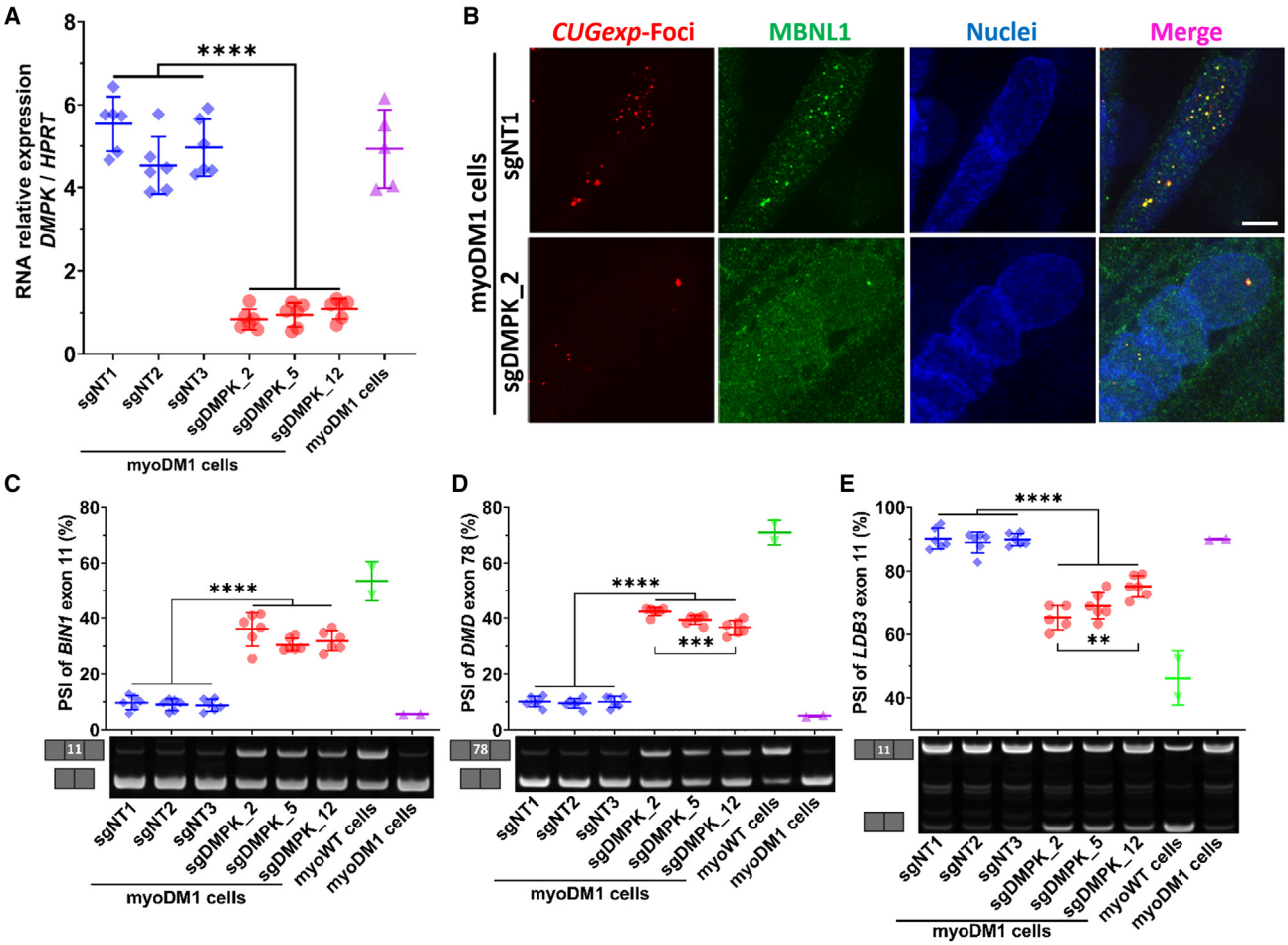

Figure 2. Correction of DM1 hallmarks by *DMPK*-promoter silencing with CRISPRi in DM1 patient-derived myotubes

(A) *DMPK* RNA quantification by qRT-PCR in DM1 myotubes (myoDM1) treated with the guides targeting the *DMPK* promoter (sgDMPK_2, _5, and _12) compared with non-target guides (sgNT1 to 3). The values of non-treated DM1 cells are displayed as references. The relative *DMPK* mRNA levels were normalized to the *HPRT* housekeeping gene. Statistics: one-way ANOVA followed by *post hoc* Tukey test for relative *DMPK* RNA level. ****$p < 0.0001$. Data are shown as the mean ± SD, n = 6 replicate transductions. (B) Observations of the nuclear relocalization of the MBNL1 protein alongside the reduction of the *CUGexp* foci in DM1 myotubes treated with sgDMPK_2 targeting the *DMPK* promoter versus the non-target guide, sgNT1. The foci were detected by FISH (in red), MBNL1 proteins were labeled by immunofluorescence (in green), and nuclei were visualized by DAPI (in blue). A Nikon Ti2 confocal microscope and a Yokogawa CSU-W1 spinning disk were used at 100× original magnification. Scale bar, 10 μm. (C–E) Correction of splicing defects by *DMPK* silencing in DM1 myotubes (myoDM1). The level of exon inclusion corresponding to the percentage splice in (PSI) index for *BIN1* exon 11 (C), *DMD* exon 78 (D), and *LDB3* exon 11 (E) was determined for DM1 myotubes expressing guides targeting the *DMPK* promoter (sgDMPK_2, _5, and _12) or non-target guides (sgNT1 to 3) by RT-PCR followed by gel electrophoresis. The values of non-treated DM1 or WT (myoWT) cells are added as references. Representative electrophoretic profiles are displayed below the charts. Statistics: one-way ANOVA followed by *post hoc* Tukey tests; **$p < 0.01$; ***$p < 0.001$; ****$p < 0.0001$. Data are shown as the mean ± SD, n = 6 replicate transductions.

demonstrated a normalization of this global electrophysiological defect in treated DM1 cells.

Globally, the repression of the *DMPK* promoter using CRISPRi leads to the normalization of a cellular physiological parameter in treated DM1 cells.

Transcriptomic specificity of *DMPK*-promoter targeting by CRISPRi in human muscle cells

A potential threat for the therapeutic strategies in development is a lack of specificity that can possibly lead to *in vivo* toxicity. To determine the specificity of our *DMPK*-promoter targeting approach through CRISPRi, we performed an additional transcriptomic analysis of differentiated myoWT cell lines expressing sgNT1, sgDMPK_2, or sgDMPK_5 generated like the previous myoDM1 cell lines (Figure S1A). Unaffected WT cells were used to distinguish off-target effects from expression modifications due to *CUGexp-DMPK* mRNA level changes in treated DM1 cells (Figure 3C).

Differential gene expression analysis between sgNT1- and sgDMPK_2-treated WT cells revealed that only the expression of the CRISPRi-targeted *DMPK* gene was significantly changed (log2 FC = −1.22;

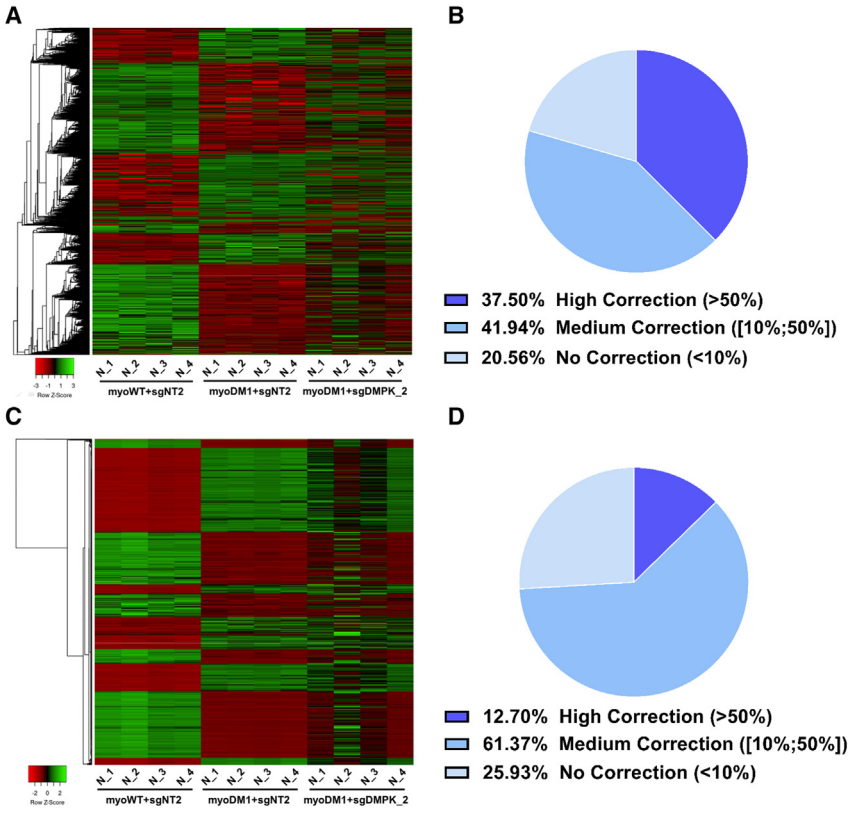

Figure 3. Global transition of DM1 patient-derived myotubes toward normal transcriptomic profile by *DMPK*-promoter inhibition through CRISPRi

(A and C) Heatmaps of the genome-wide transcriptomic profiling of DM1 myotubes (myoDM1) expressing sgDMPK_2, targeting the *DMPK* promoter, compared with WT (myoWT) and DM1 cells treated with non-target guide, sgNT2. The differential events in DM1 myotubes (myoWT + sgNT2 versus myoDM1 + sgNT2) are represented by hierarchical clustering at the splicing (A, FDR ≤ 0.05, ΔPSI ≥ |0.15|) and gene expression levels (C, FDR ≤ 0.05, log2 FC ≥ |1|); n = 4 replicate transductions. (B and D) Pie charts showing the level of correction induced by the *DMPK*-silencing strategy for transcriptomic events deregulated in DM1 (myoWT + sgNT2 versus myoDM1 + sgNT2) at the splicing (B) and gene expression levels (D). These improvements were divided into three categories: no to low correction for changes <10%, medium correction for changes within the range of 10%–50%, and high correction for changes >50%; n = 4 replicate transductions.

adjusted [adj.] p = 2.17×10^{-39}; Figures 5A and 5B and Table S2). Moreover, this analysis also confirmed the 80% reduction in *DMPK* mRNA levels previously quantified by qRT-PCR (Figures 1D and S1C–S1G). Interestingly, the *DMPK* antisense transcript, *DM1-AS* (log2 FC = −0.44; adj. p = 2.09×10^{-4}), was the single other gene showing a modified expression while not reaching the log2 FC ≥ |1| threshold. These findings were further confirmed by a second analysis of WT cells expressing sgDMPK_5 (Figures 5C and 5D and Table S2). As previously, *DMPK* was the only transcript significantly downregulated (log2 FC = −1.44; adj. p = 3.16×10^{-57}) according to our analysis threshold (log2 FC ≥ |1| and adj. p ≤ 0.05). In addition to *DM1-AS* (log2 FC = −0.42; adj. p = 4.14×10^{-4}), four other transcripts were also affected, albeit with a limited variation in expression (log2 FC ≤ |1|): *SDHAP3* (succinate dehydrogenase complex flavoprotein subunit A pseudogene 3; log2 FC = −0.67; adj. p = 4.05×10^{-13}), *ACTN2* (alpha-actinin-2; log2 FC = −0.47; adj. p = 1.70×10^{-5}), *AC026412.1* (log2 FC = −0.39; adj. p = 6.02×10^{-4}), and *AC116533.1* (log2 FC = +0.37; adj. p = 0.043).

Altogether, these results confirmed the inherent specificity of our *DMPK*-promoter-targeting CRISPRi approach using either sgDMPK_2 or sgDMPK_5 RNA guides.

DISCUSSION

In this proof-of-concept study, we provided evidence that the repression of the *DMPK* promoter through the CRISPRi system offers a relevant and promising strategy to specifically silence the expression of the pathogenic *CTGexp-DMPK* gene causing DM1. We showed that specific *DMPK* sgRNAs driving a dCas9 fused to a KRAB repressor domain allow effective decrease (up to 80% for the sgDMPK_2) in the level of *CUGexp-DMPK* transcripts, in association with a reduction in the number of toxic *CUGexp* RNA foci. Consequently, free and functional MBNL1 is released into the nucleoplasm of treated DM1 muscle cells, resulting in the correction of MBNL1-dependent alternative splicing events, such as *DMD* exon 78, *BIN1* exon 11, and *LDB3* exon 11, which are misregulated in DM1. These levels of *CUGexp-DMPK* mRNA reduction and missplicing corrections following *DMPK*-promoter silencing by CRISPRi are globally similar to the strategies tested in equivalent DM1 muscle cell models.[27,40,46–48] To date, these have included approaches aiming to either reduce the level of the toxic *DMPK* RNA, at the DNA level with the dCas9-$(CAG)_6$ gene therapy[27] and at the RNA level with the gapmer ISIS 486175,[40] or block the sequestration of MBNL proteins with U7snRNA-$(CAG)_{15}$[39,46] and steric blocking CUG-ASO.[39,47] DM1 cells in which CTG expansions were excised with the CRISPR-Cas9 gene editing tool displayed an almost complete reversal of DM1 defects. Along with this remarkable therapeutic efficacy, a low proportion of edited cells was, however, observed *in vitro* and *in vivo*.[26,49] RNA sequencing demonstrated that the overall transcriptome of DM1 muscle cells expressing our CRISPRi system was corrected at both gene expression and alternative splicing levels. Moreover, GO term enrichment analysis also showed that altered cellular functions in DM1 muscle cells, such as ionic membrane currents, were improved. Impaired potassium and sodium transmembrane currents were previously described in skeletal muscle cells from DM1 patients,[50–55] and we showed that the electrical membrane resistance of DM1 muscle cells is altered

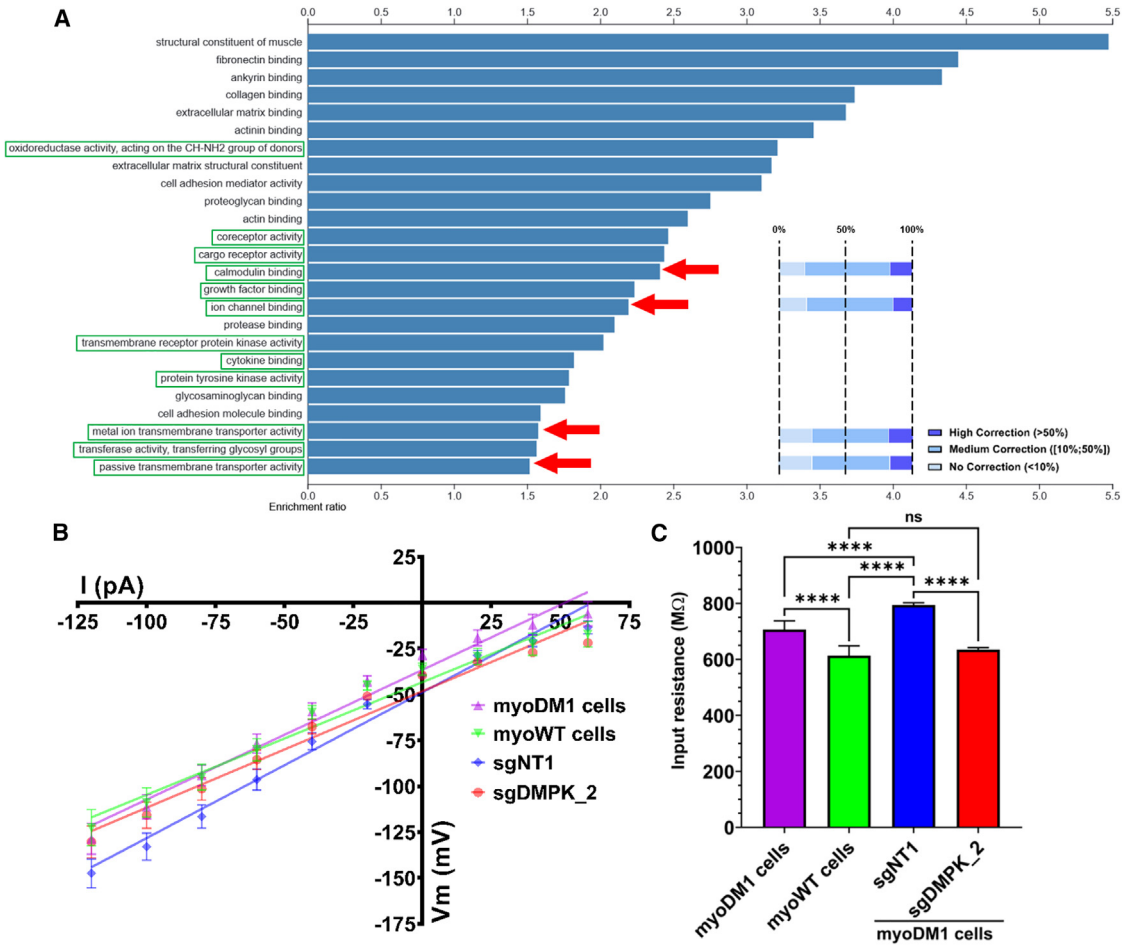

Figure 4. Normalization of a physiological parameter by CRISPRi targeting the *DMPK* promoter in DM1 patient-derived myotubes

(A) GO term analysis using the WebGestalt online tool from the 1,913 differentially expressed genes deregulated in DM1 myotubes (myoDM1 + sgNT2 versus myoWT + sgNT2; FDR ≤ 0.05; log2 FC ≥ |1|). The green boxes outline non-structural functions, while the red arrows highlight molecular functions related to cellular ionic currents. The level of correction induced by *DMPK* silencing with sgDMPK-2 for GO terms related to ionic current is indicated on the chart. The correction was distributed into three categories: no to low correction for changes <10%, medium correction for changes in the range of 10%–50%, and high correction for changes >50%; n = 4 replicate transductions. (B and C) The membrane potential (Vm)-input current (I) relationship curve of myotubes under different treatment conditions was determined by whole-cell patch-clamp recordings in the current clamp configuration. The slope corresponds to the electrical membrane resistance of the recorded cells by Ohm's law. Membrane resistance values measured in patch-clamp recordings from (B) are represented as histograms in (C). Statistics: one-way ANOVA followed by *post hoc* Tukey tests; ****$p < 0.0001$. Data are shown as the mean ± SD, n = 12–16 cells among the six replicate transductions.

compared with WT muscle cells. This physiological parameter was normalized in treated DM1 muscle cells, confirming the functional benefits of transcriptome regulation at both cellular and functional levels.

Remarkably, almost no change in gene expression was detected by RNA sequencing of WT muscle cells expressing the dCas9-KRAB in combination with the sgDMPK_2 or the sgDMPK_5, demonstrating an unprecedented specificity of the *DMPK*-promoter targeting strategy by CRISPRi in a human genomic context among the therapeutic strategies developed for DM1. This is likely provided by the core concept of the *DMPK*-promoter targeting, especially by the CRISPRi technology, which displays very low levels of off-targets in various *in vitro* and *in vivo* models.[31] Indeed, the DNA binding of the inhibitory agent outside the very restricted promoter/enhancer region does not induce any transcriptional effect,[30,56] as confirmed by the highly specific repression of the mouse *mapt* promoter targeted with a relative genomic inhibitor as a zinc-finger-KRAB protein.[57] Furthermore, off-target effects associated with gene-editing strategies and leading to irreversible genome modifications are not expected to occur with the promoter-silencing approach by CRISPRi because it is based on the use of a driven inhibitor devoid of endonuclease activity.[58] The *DMPK*-promoter silencing strategy does not allow discrimination between the *CTGexp-DMPK* and the *normal-DMPK* allele, thus leading to the repression of both *CUGexp-DMPK* and *normal-DMPK* transcripts (Figures S1C–S1G). The DMPK protein is already

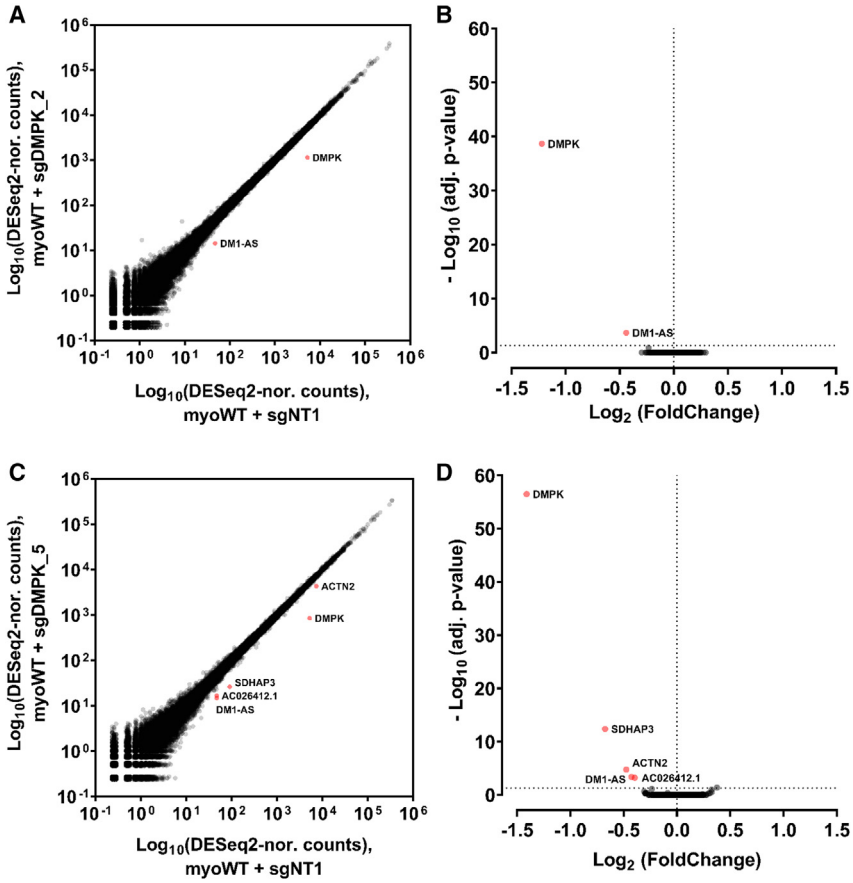

Figure 5. Transcriptomic specificity of the *DMPK*-promoter-inhibitory strategy by CRISPRi in myotubes derived from an unaffected individual

(A–D) The overall specificity of *DMPK*-promoter silencing by CRISPRi was assessed by RNA-sequencing analysis of gene expression in unaffected myotubes (myoWT). Differential genome-wide expression profiling in WT cells treated with a guide targeting *DMPK* (y axis, A for sgDMPK_2 and C for sgDMPK_5) compared with WT cells treated with a non-target guide (x axis, sgNT1) as well as the respective volcano plots (B and D) is represented. The highlighted transcripts are characterized by a significant expression modification with an adjusted $p < 0.05$; n = 4 replicate transductions.

reduced by 50% in DM1 cells, since *CUGexp-DMPK* transcripts are retained in the nucleus.[38] The silencing of the normal *DMPK* allele will lead to a larger or almost complete DMPK protein deficiency. At the molecular level, the lack of common modifications of gene expression in WT cells expressing sgDMPK_2 and sgDMPK_5 indicates that the *DMPK* gene did not affect expression of other genes. This observation could be explained by the primary function of DMPK protein, which is a serine/threonine kinase.[59] The DMPK protein thus affected post-translational modifications. In addition, the serine/threonine kinase family of proteins includes more than 63 kinases.[59] Consequently, a functional compensation by at least one of these kinases likely occurs in human myotubes. This hypothesis could be put into perspective by observations in the *Dmpk-KO* mouse model, which either showed no phenotype or could develop late-onset progressive myopathy and cardiac conduction changes.[60–63] Moreover, near-complete degradation of the *Dmpk* transcripts by RNase H1-dependent antisense oligonucleotides is well tolerated in adult WT mice and monkeys without muscle or cardiac abnormalities.[64,65] Our CRISPRi approach mimics this last condition, suggesting that the therapeutic benefit of repressing the *DMPK* gene is probably higher than the potential adverse effects caused by a reduction in DMPK protein in the adult tissue of DM1 patients. Alternatively, some strategies propose targeting directly the expanded repeats at the genomic or transcriptomic level by dCas9 protein[27] or blocking ASO, respectively.[66] While these approaches allow a partial preservation of the WT *DMPK* transcript, the targeting of the expanded tract also affects, in any case, off-target transcripts containing a physiological number of CUG triplets[67] or not.[27] In addition, the length of the expanded CTG tract is inherently unstable, leading to further expansion and heterogeneity of CTG expansion across tissues during the lifespan of patients.[68] Therapeutic approaches targeting the expanded repeats at the DNA or RNA level may thus become less effective over time depending on the tissue. Furthermore, RNA interference or strategies designed to block the deleterious binding of MBNL proteins to the expanded CUG repeats must contend with the constant expression of the mutated transcripts. In contrast, the targets of our strategy, the two alleles of the *DMPK* gene, are low and constant across time and cell types, which probably potentiates the global efficacy of the *DMPK*-promoter targeting approach in all DM1 patients.

Finally, *DMPK* is the sole gene that is significantly repressed by the *DMPK*-promoter silencing approach. Interestingly, a reproducible effect on the *DM1-AS* gene was also revealed by RNA-sequencing data from cells expressing either sgDMPK_2 or sgDMPK_5. The *DM1-AS* expressed at the DM1 locus an antisense RNA containing CAG expanded repeats in DM1 cells and was associated with the production of cytotoxic homopolymeric expansion proteins through repeat-associated non-ATG (RAN) translation.[69] Further studies will determine whether the repression of the *CTGexp-DMPK* promoter affects the production of RAN proteins, although the contribution of RAN peptides in DM1 pathophysiology is not fully understood, in contrast to other microsatellite expansion pathologies.[70]

Due to its specificity and efficacy, the *DMPK*-silencing approach by CRISPRi is therefore a valuable therapeutic strategy that expands the therapeutic toolbox available to treat DM1 disease. This alternative approach needs to be further validated in a DM1 mouse model.

For this purpose, the delivery of the CRISPRi system is critical to the success of such gene therapy. Among several delivery strategies, recombinant adeno-associated virus (AAV) vectors (rAAVs) are the most suitable, given the high transduction efficacy on a broad range of tissues, including the skeletal muscles or the CNS,[71] affected in DM1. However, the CRISPRi expression cassette (sgRNA and dSpCas9/KRAB) used in this study exceeds by 0.8 kb the packaging capacity of rAAV, which is limited to 4.5 kb.[72] Optimizations are therefore needed to overcome this limitation and further develop the *DMPK*-promoter silencing approach.

MATERIALS AND METHODS

Cell culture

Myoblasts from unaffected female and male individuals for primary (myoWT_2) and immortalized WT cells (clone 48, myoWT), respectively, as well as a DM1 female patient with 2,600 CTG repeats for primary and immortalized DM1 cells (immortalized: clone 6, myoDM1), provided by the human cell immortalization facility at the Myology Institute, were described previously.[39,73–75] These cells were previously validated to assess different therapeutic approaches in DM1.[39] The myogenic cells were incubated at 37°C, 5% CO_2, in proliferation medium consisting of a mix of M199 Earle's salts:DMEM (1:4 ratio; Gibco) supplemented with 20% fetal bovine serum (FBS) (Gibco), 50 μg/mL gentamycin (Gibco, 15750037), 25 μg/mL fetuin (Merk, F2379), 5 μg/mL insulin (Gibco, 12585014), 0.2 μg/mL dexamethasone (Merk, D4902), 5 ng/mL epidermal growth factor (EGF) (Gibco, PHG0311L), and 0.5 ng/mL basic fibroblast growth factor (bFGF) (Gibco, PHG0024). Myogenic differentiation was induced by switching confluent cell cultures in Matrigel Growth Factors Reduced-coated Petri dishes (150 μg/mL, Matrigel GFR, 354230, Corning) to differentiation medium characterized by a mix of M199 Earle's salts:DMEM (1:4 ratio; Gibco) supplemented with 2% B27 (Gibco, 17504044), 100 μg/mL human apo-transferrin (Merck, T2036), 50 μg/mL gentamycin (Gibco, 15750037), and 10 μg/mL insulin (Gibco, 12585014). Primary and immortalized WT myotubes were differentiated for 3 days, while immortalized DM1 cells were extended to 6 days, unless otherwise indicated. The medium was changed to fresh differentiation medium every 3 days.

The absence of mycoplasmas in cell culture was confirmed by the GIGA Viral Vectors platform with MycoAlert PLUS Mycoplasma Detection Kit (Lonza, LT07-710).

Plasmids and design of sgRNAs

Due to the puromycin-resistant status of immortalized myoblasts,[39] we switched the puromycin-resistance gene from pLV hU6-sgRNA hUbC-dCas9-KRAB-T2a-Puro lentiviral plasmid (a gift from Charles Gersbach; Addgene plasmid 71236) digested with AscI (R0558, NEB) and AgeI-HF (R3552, NEB) restriction enzymes, to a blasticidin-resistance gene using NEBuilder HiFi DNA Assembly (E2621, NEB). Consequently, the new plasmid contains the blasticidin-resistance gene as well as an all-in-one CRISPRi system including sgRNA[29] and humanized nuclease-deficient Cas9 (D10A and H840A mutations) from *Streptococcus pyogenes* fused to a human KRAB domain from the human zinc-finger protein ZNF10 (KOX1).[34]

For the design of the sgRNA, the TSS of the human *DMPK* gene was identified at chr19:46,285,815 (GRCh37/hg19) using the online database FANTOM5.[76,77] Guides of 20 bp with a Protospacer Adjacent Motif (PAM) sequence of 3′-NGG in the genomic window at −50 and +300 bp around the TSS of the targeted *DMPK* gene[30,78] were considered. Online design tools such as E-CRISP,[79] CRISPR-ERA,[80] CRISPRscan,[81] CHOPCHOP,[82] CCTOP,[83] and the sgRNA design tool from the Broad Institute[84,85] were used to generate different sgRNAs (denoted sgDMPK, Table 1). For negative controls, sgRNAs that do not target the human genome (denoted sgNTs) were used in all experiments. sgNT1 and sgNT2 came from Sigma-Aldrich, while sgNT3 was from Origene. These scramble sgRNAs were classically used in the literature. The sgDMPKs and sgNTs were individually cloned into the new pLV hU6-sgRNA hUbC-dCas9-KRAB-T2a-blasti lentiviral plasmid as described previously.[86] Briefly, the top and bottom strands of oligonucleotides with sticky ends of the BsmBI enzyme on their 5′ termini were chemically synthesized at IDT (Integrated DNA Technologies). The oligonucleotides were phosphorylated and annealed in a thermal cycler using the following program: 37°C for 30 min, 95°C for 5 min, and ramp down to 25°C at 5°C/min. Then, pLV hU6-sgRNA hUbC-dCas9-KRAB-T2a-blasti were digested by BsmBI restriction enzyme (Thermo Scientific FastDigest Esp3I) and ligated with each sgRNA. The insertions of the sgRNAs were validated by Sanger sequencing.

Lentiviral vector production and myoblast transduction

Integrative lentiviral vectors were generated by the GIGA Viral Vectors platform. Briefly, Lenti-X 293T cells (Clontech, 632180) were co-transfected with pLV hU6-sgRNA hUbC-dCas9-KRAB-T2a-blasti including a specific sgRNA, a pSPAX2 (Addgene, Cambridge, MA, USA), and a VSV-G-encoding vector.[87] Viral supernatants were collected 48, 72, and 96 h post-transfection, filtered (0.2 μm), and concentrated 100× by ultracentrifugation. The lentiviral vectors were then titrated with a qPCR Lentivirus Titration (Titer) Kit (ABM, LV900, Richmond, BC, Canada). Next, the primary or immortalized myoblasts were transduced at MOI of 10 and the primary cells were transduced at the earliest passage. The subsequent polyclonal population was selected with blasticidin (11 μg/mL, ant-bl-1, Invivogen) to produce stable cell lines expressing both the dCas9/KRAB protein and the respective sgRNA.

Combined RNA fluorescence *in situ* hybridization and MBNL1 staining by immunofluorescence as well as image analysis

FISH experiments were done as previously described using a Cy3-labeled peptide nucleic acid $(CAG)_5$ probe (Eurogentec) to label nuclear foci.[88] Briefly, myoblast cells were grown and differentiated in Matrigel GFR-coated ibidi plates (μ-Plate 24 well black, ibiTreat, 82406, Ibidi). Then, the cells were washed in PBS and fixed in 4% paraformaldehyde solution (PFA). After fixation, the cells were dehydrated and permeabilized overnight in EtOH 70% at 4°C. The next day, the cells were rehydrated in PBS + 5 mM $MgCl_2$ and

sequentially incubated with 2 nM Cy3-labeled $(CAG)_5$ probe in hybridization buffer (40% formamide, 2× SSC [saline sodium citrate UltraPure 20×, 15557044, Invitrogen], 0.2% BSA [bovine serum albumin acetylated, AM2614, Invitrogen]) at 37°C. Then, the cells were washed twice in PBS + 0.1% Tween 20 (P2287, Sigma-Aldrich) at room temperature and 45°C sequentially. In the case of combined MBNL1 staining by a coimmunofluorescence (co-IF) assay, the cells were permeabilized again in PBS/1.5% Triton X-100 (Sigma-Aldrich) buffer and then blocked in PBS-Tween 3% BSA (albumin fraction V, 8076.4, Roth) buffer. The MBNL1 staining was carried out with a mouse monoclonal antibody, anti-MBNL1 (1:100, MB1a clone 4A8 gift, from G.E. Morris, DHSB) followed by a secondary Alexa Fluor 488-conjugated goat anti-mouse (1:500, Life Technologies) antibody. The nuclear counterstaining was done with 2 μg/mL DAPI for all assays before coverslips were mounted with ProLong Diamond antifading mounting medium (P36965, Molecular Probes) and kept at 4°C.

For FISH-IF assays, fluorescence images from primary cells were taken with a Zeiss Axio Observed inverted microscope at magnification factor ×63 for primary cells, whereas confocal images from immortalized cells were realized with a Nikon Ti2 microscope equipped with a motorized stage and a Yokogawa CSU-W1 spinning disk head coupled with a Prime 95 sCMOS camera (Photometrics) at magnification factor ×100. The image acquisition for FISH alone from immortalized cells was done with a Zeiss LSM 880 AiryScan confocal microscope (Zeiss, Germany) at magnification factor ×40 on 12 stacks. An image for FISH included typically several hundred nuclei. Next, the automated quantification of the global nuclear focus density was performed using the image analysis toolbox of MATLAB R1018a (MathWorks) software and custom scripts. Briefly, the maximal projections of the stacked images of each color channel (foci, red, and DAPI, blue) were denoised using a median filter and binarized using an automatic threshold by the Otsu method.[89] Finally, the global nuclear focus density, defined as the total area of foci that colocalized with DAPI divided by the total area of DAPI, was determined.

Total RNA extraction

A standard total RNA extraction on a silica column (NucleoSpin RNA Plus kit, 740984, Machery-Nagel) was used for experiments involving only immortalized WT cell lines; otherwise, total RNAs from all cells were extracted using liquid/liquid extraction by phenol-guanidinium thiocyanate/chloroform (Qiazol, 79306, Qiagen). The cell lysate was incubated with the phenol-guanidinium thiocyanate solution at 55°C with stirring at 1,000 rpm for 20 min to allow optimal extraction of expanded *DMPK* transcripts,[90,91] except for the RNA sequencing used for the correction study, where a standard Qiazol extraction was done. Thereafter, the total RNA solution from the two RNA extraction processes was treated with DNase (TURBO DNA-free kit, AM1907, Invitrogen). RNA concentrations were determined using a NanoDrop (Thermo Scientific). Finally, the DNA-free RNA solution was stored at −80°C.

qRT-PCR analysis for *DMPK* gene expression

One microgram of DNA-free total RNA was reverse transcribed using the SuperScript IV First-Strand synthesis system (15327696, Invitrogen) according to the manufacturer's instructions. To quantify the gene expression, qPCR was performed with a SYBR green kit (Takyon, UF-NSMT-B0710, Eurogentec) and a LightCycler 480 (Roche) according to the manufacturer's instructions. The PCR program was composed of a 5-min denaturation step, followed by 45 cycles of 95°C denaturation for 10 s, 60°C annealing for 10 s, and 72°C extension for 10 s, as well as a melting curve. Ct values were determined by the second derivative method with the LightCycler 480 analysis software. Then, the $2^{-\Delta\Delta Ct}$ method[92] was used to determine the relative expression level of each gene with *HPRT* (UniProt: P00492, hypoxanthine-guanine phosphoribosyltransferase), *TBP* (UniProt: P20226, TATA box binding protein), and *RPL0* (60S ribosomal protein L0) as human reference genes.[93] The primers used are identified in Table 2.

RT-PCR analysis for alternative splicing

One microgram of DNA-free total RNA was reverse transcribed using SuperScript IV First-Strand synthesis system (15327696, Invitrogen) according to the manufacturer's protocol. To analyze alternative splicing, 1 μL of cDNA preparation was amplified by PCR according to the manufacturer's instructions (OneTaq Hot Start 2× master mix with standard buffer, M0484, NEB). Thereafter, PCR products were resolved by electrophoresis on 10% polyacrylamide gels (bis-acrylamide 29:1, solution 40%, 10001313, Fisher BioReagents) stained by GelStar (GelStar Nucleic Acid Gel Stain, LO 50535, Lonza) for immortalized cells or a QIAxcel Advanced system (Qiagen) for primary cells. The ratio of exon inclusion corresponding to the PSI index was expressed as the ratio of the densitometric intensity of the isoform containing the alternative exon relative to the total intensities of all isoform signals. Isoform signal was quantified using the ImageQuant TL (GE Lifesciences) software for gel electrophoresis and QIAxcel software otherwise. Detailed information on the primers used is provided in Table 2.

Whole-cell patch clamp for electrical membrane resistance

The physiological properties of differentiated myoblasts were investigated by whole-cell patch clamp. For this purpose, the cells were superfused with a medium mimicking the ionic composition of their physiological extracellular environment (145 mM NaCl, 4.5 mM KCl, 1 mM $CaCl_2$, 10 mM HEPES, 1 mM $MgCl_2$, and 10 mM D-glucose [pH 7.3–7], osmolarity ∼320 mOsmol/L). A borosilicate pipette (resistance of 3–5 MΩ) was pulled using a P97 puller (Sutter Instruments). It was filled with a close-to-physiological solution containing 135 mM K-$MeSO_4$, 1 mM $MgSO_4$, 0.1 mM $CaCl_2$, 2 mM Na_2ATP, 10 mM EGTA, and 10 mM HEPES (pH 7.2 using KOH), osmolarity ∼300 mOsmol/L). After reaching the whole-cell mode, membrane potentials (Vm) were recorded in current clamp and current (I) injections of variable amplitude were used to assess the input resistance (Rm) using Ohm's law, Rm = Vm/I. The protocol used consisted of steps of current of 1 s and ranging from −120 to 60 pA with 20-pA increments.

Table 2. Features of PCR primers

Designation	Orientation	Sequence	Annealing temperature	Source
F_qPCR_*HPRT*	forward	5′-GGTCAGGCAGTATAATCCAAAG-3′	60°C	Hubaux et al., 2015[94]
R_qPCR_*HPRT*	reverse	5′-AAGGGCATATCCTACAACAAAC-3′		
F_qPCR_*TBP*	forward	5′-TGCACAGGAGCCAAGAGTGAA-3′		RTprimerDB (id_2627)
R_qPCR_*TBP*	reverse	5′-CACATCACAGCTCCCCACCA-3′		
F_qPCR_*RPL0*	forward	5′-ACGGGTACAAACGAGTCCTGG-3′		this study
R_qPCR_*RPL0*	reverse	5′-GCCACAAAGGCAGATGGATCAG-3′		
F_qPCR_*DMPK*	forward	5′-GGTAGTGAAGATGAAGCAGACGG-3′		Eriksson et al., 2004[95]
R_qPCR_*DMPK*	reverse	5′-GGAAGCACGACACCTCGC-3′		
F_qPCR_*MyH3*	forward	5′-ATTGCTTCGTGGTGGACTCAA-3′		Zhang et al.[44]
R_qPCR_*MyH3*	reverse	5′-GGCCATGTCTTCGATCCTGTC-3′		
F_qPCR_*MyoG*	forward	5′-AGCGAATGCAGCTCTCACAG-3′		this study
R_qPCR_*MyoG*	reverse	5′-CATCTGTAGGGTCAGCCGTG-3′		
F_*BIN1* exon 11	forward	5′-AGAACCTCAATGATGTGCTGG-3′	53°C	Arandel et al.[48]
R_*BIN1* exon 11	reverse	5′-CGTGGTTGACTCTGATCTCGG-3′		
F_*DMD* exon 78	forward	5′-TTAGAGGAGGTGATGGAGCA-3′	50°C	
R_*DMD* exon 78	reverse	5′-GATACTAAGGACTCCATCGC-3′		
F_*MBNL1* exon 5	forward	5′-GCTGCCCAATACCAGGTCAAC-3′	55°C	
R_*MBNL1* exon 5	reverse	5′-TGGTGGGAGAAATGCTGTATGC-3′		
F_*LDB3* exon 11	forward	5′-CCCTGATGAAGAAGCTCTGC-3′	54°C	this study
R_*LDB3* exon 11	reverse	5′-CGGATGCTGGCAGTGGTGAC-3′		
F_*SORBS1* exon 25	forward	5′-CGGAAGAATTTATTCGAAGACG-3′	49°C	Jauvin et al.[40]
R_*SORBS1* exon 25	reverse	5′-TGTAGGTGCGTGGGAAGATT-3′		

Transcriptome analysis by RNA sequencing

The RNA sequencing was performed by the GIGA-Genomics platform (GIGA, ULiège). DNA-free total RNA quality was checked via Bioanalyzer 2100 (Agilent), ensuring RIN values greater than 9.2. Thereafter, libraries were generated using a TruSeq Stranded mRNA Library Prep Kit (20020595, Illumina), where poly(A)$^+$ RNAs are isolated by poly(A) selection and pooled together by multiplexing them using barcoded adapters. The pooled libraries were then sequenced in the Illumina NovaSeq 6000 sequencing system as 150-bp paired-end reads with at least 25 million raw reads per sample for the specificity study or 80 million reads per sample for the correction study.

For the correction study, the quality of raw reads was checked by FastQC v.0.11.8 and a trimming was applied with Cutadapt[96] with a minimum length of 75 bp and an error rate of 0.1. Then, 86.3%–90.3% of raw reads were uniquely aligned to the GRCh38 human genome by STAR v.2.7.5a,[97] annotated using the Gencode reference of human genome v.39 and counted on the gene level by HTSeq-count v.0.12.4[98] in overlap resolution mode "union" on the reverse strand. The alternative splicing analysis was performed using rMATS turbo v.4.1.1,[99] while the differential gene expression analysis was performed with DESeq2 v.1.34.0,[100] based on a negative binomial generalized linear model and Wald test for significance, from previous annotated and counted reads. The heatmaps were generated by hierarchical clustering (metric, Euclidian distance; linkage method, average) using the Heatmapper online tool[101] from the differential events (FDR $\leq$ 0.05; ΔPSI $\geq$ |0.15|) of myoDM1 + sgNT2 versus myoWT + sgNT2 at the splicing (FDR $\leq$ 0.05; ΔPSI $\geq$ |0.15|; 2,432 splicing events) and gene expression levels (FDR $\leq$ 0.05; log2 FC $\geq$ |1|; 1,913 gene-expression events). The GO term enrichment analysis was realized with the WebGestalt online tool (enrichment method, ORA; enrichment categories, no redundant geneontology molecular function; reference set, genome)[102] based on gene expression changes identified in DESeq2 between DM1 + sgNT2 and WT + sgNT2 conditions (FDR $\leq$ 0.05; log2 FC $\geq$ |1|; 1,913 gene-expression events). Scripts of the correction analysis are publicly available at https://github.com/mariakondili/DM1_vs_sgDMPK/.

For the specificity study, high quality of raw reads was shown by FastQC v.0.11.8. Subsequently, any trimming was done. Thereafter, 84.8%–91.4% of raw reads were uniquely aligned to the GRCh38 human genome by STAR v.2.6.1d.[97] Uniquely aligning paired sequences were annotated using Ensembl release 97[103] and counted by featureCounts v.1.6.4.[104] Finally, differential expression analysis was performed with DESeq2 v.1.29.4.[100]

To correct the effect of multiple testing, an adjusted p value (adj. p or FDR) was determined by Benjamini and Hochberg correction (FDR $\leq$ 0.05 used as cutoff for considering a gene significant).[100,105] Complete raw data generated from RNA sequencing were deposited in the European Nucleotide Archive (accession no. PRJEB60168) of the European Bioinformatics Institute.

Statistical analysis

All group data are shown as the mean ± SD. Between experimental groups, the comparison was performed by Student's t test or one-way ANOVA followed by Tukey post-test using Prism 8 software (GraphPad Software). Differences between groups were considered significant when $p < 0.05$ (*$p < 0.05$, **$p < 0.01$, ***$p < 0.001$, ****$p < 0.0001$). To simplify some figures, the statistical significance was specified by *test *post hoc* versus sgNT1, §test *post hoc* versus sgNT2, and ¥test *post hoc* versus sgNT3.

Graphic representations

All charts, except heatmaps and representation of GO terms generated respectively from Heatmapper and WebGestalt online tools, were realized with Prism 8 software (GraphPad Software).

DATA AVAILABILITY

Complete raw data generated from RNA sequencing were deposited in the European Nucleotide Archive of the European Bioinformatics Institute under accession no. PRJEB60168. Other datasets generated during the current study are available from the corresponding authors on reasonable request.

SUPPLEMENTAL INFORMATION

Supplemental information can be found online at https://doi.org/10.1016/j.omtn.2023.05.007.

ACKNOWLEDGMENTS

The authors thank the human cell immortalization facility of the Myology Institute (Paris, France) as well as the GIGA technological platforms for support. In particular, the authors are grateful to François Giroulle, Alexandre Hego, Latifa Karim, Sandra Ormenese, Wouter Coppieters, Alexandra Revnic, Arnaud Lavergne, Raafat Stephan, and Stephen Freeman for their technical expertise and engagement, as well as Mario Gomes-Pereira, Marc Bitoun, and Geneviève Gourdon for their advice. This work was supported by the Fonds National de la Recherche Scientifique (FNRS, FRIA grant), The Myotonic Dystrophy Foundation and Wyck Foundations (2018 PhD trainee fellowship in Myotonic Dystrophy), the Association Belge contre les Maladies Neuro-Musculaires (ABMM; call 2019–2020), and the Fondation Léon Fredericq (FLF). F.P. was supported by fellowships of the Fonds National de la Recherche Scientifique, The Myotonic Dystrophy Foundation, and Wyck Foundations. V.S. is a full professor at ULiege, while L. Willems is a research director at the FNRS and A.F.K. is a research scientist at INSERM.

AUTHOR CONTRIBUTIONS

Conceptualization, F.P.; methodology, F.P.; software, S.B. and M.K.; formal analysis, F.P. and K.J.; investigation, F.P., L. Weidong, A.F.K., H.G., and L.M.; resources, E.D.V., D.F., and A.F.K.; writing – original draft, F.P.; writing – review & editing, F.P., A.F.K., D.F., V.S., and L. Willems; visualization, F.P. and A.F.K.; supervision, A.F.K., N.A.G., L. Willems, and V.S.; project administration, V.S. and L. Willems; funding acquisition, F.P.

DECLARATION OF INTERESTS

The authors declare no competing interests.

REFERENCES

1. Gourdon, G., and Meola, G. (2017). Myotonic dystrophies: state of the art of new therapeutic developments for the CNS. Front. Cell. Neurosci. *11*, 101–114. https://doi.org/10.3389/fncel.2017.00101.

2. Wenninger, S., Montagnese, F., Schoser, B., and Wenninger, S. (2018). Core clinical phenotypes in myotonic dystrophies. Front. Neurol. *9*, 303–309. https://doi.org/10.3389/fneur.2018.00303.

3. Theadom, A., Rodrigues, M., Roxburgh, R., Balalla, S., Higgins, C., Bhattacharjee, R., Jones, K., Krishnamurthi, R., and Feigin, V. (2014). Prevalence of muscular dystrophies : a systematic literature Review. Neuroepidemiology *43*, 259–268. https://doi.org/10.1159/000369343.

4. Johnson, N.E., Butterfield, R.J., Mayne, K., Newcomb, T., Imburgia, C., Dunn, D., Duval, B., Feldkamp, M.L., and Weiss, R.B. (2021). Population-based prevalence of myotonic dystrophy type 1 using genetic analysis of statewide blood screening program. Neurology *96*, e1045–e1053. https://doi.org/10.1212/WNL.0000000000011425.

5. Brook, J.D., McCurrach, M.E., Harley, H.G., Buckler, A.J., Church, D., Aburatani, H., Hunter, K., Stanton, V.P., Thirion, J.-P., Hudson, T., et al. (1992). Molecular basis of myotonic dystrophy: expansion of a trinucleotide (CTG) repeat at the 3' end of a transcript encoding a protein kinase family member. Cell *69*, 385–808. https://doi.org/10.1016/0092-8674(92)90418-C.

6. De Antonio, M., Dogan, C., Hamroun, D., Mati, M., Zerrouki, S., Eymard, B., Katsahian, S., and Bassez, G.; French Myotonic Dystrophy Clinical Network (2016). Unravelling the myotonic dystrophy type 1 clinical spectrum: a systematic registry-based study with implications for disease classification. Rev. Neurol. *172*, 572–580. https://doi.org/10.1016/j.neurol.2016.08.003.

7. Hale, M.A., Johnson, N.E., and Berglund, J.A. (2019). Repeat-associated RNA structure and aberrant splicing. Biochim. Biophys. Acta. Gene Regul. Mech. *1862*, 194405. https://doi.org/10.1016/j.bbagrm.2019.07.006.

8. Taneja, K.L., McCurrach, M., Schalling, M., Housman, D., and Singer, R.H. (1995). Foci of trinucleotide repeat transcripts in nuclei of myotonic dystrophy cells and tissues. J. Cell Biol. *128*, 995–1002. https://doi.org/10.1083/jcb.128.6.995.

9. Jain, A., and Vale, R.D. (2017). RNA phase transitions in repeat expansion disorders. Nature *546*, 243–247. https://doi.org/10.1038/nature22386.

10. Goers, E.S., Purcell, J., Voelker, R.B., Gates, D.P., and Berglund, J.A. (2010). MBNL1 binds GC motifs embedded in pyrimidines to regulate alternative splicing. Nucleic Acids Res. *38*, 2467–2484. https://doi.org/10.1093/nar/gkp1209.

11. Osborne, R.J., Lin, X., Welle, S., Sobczak, K., O'Rourke, J.R., Swanson, M.S., and Thornton, C.A. (2009). Transcriptional and post-transcriptional impact of toxic RNA in myotonic dystrophy. Hum. Mol. Genet. *18*, 1471–1481. https://doi.org/10.1093/hmg/ddp058.

12. Kanadia, R.N., Johnstone, K.A., Mankodi, A., Lungu, C., Thornton, C.A., Esson, D., Timmers, A.M., Hauswirth, W.W., and Swanson, M.S. (2003). A muscleblind knockout model for myotonic dystrophy. Science *302*, 1978–1980. https://doi.org/10.1126/science.1088583.

13. Lee, K.Y., Li, M., Manchanda, M., Batra, R., Charizanis, K., Mohan, A., Warren, S.A., Chamberlain, C.M., Finn, D., Hong, H., et al. (2013). Compound loss of muscleblind-like function in myotonic dystrophy. EMBO Mol. Med. *5*, 1887–1900. https://doi.org/10.1002/emmm.201303275.

14. Thomas, J.D., Sznajder, Ł.J., Bardhi, O., Aslam, F.N., Anastasiadis, Z.P., Scotti, M.M., Nishino, I., Nakamori, M., Wang, E.T., and Swanson, M.S. (2017). Disrupted prenatal RNA processing and myogenesis in congenital myotonic dystrophy. Genes Dev. *31*, 1122–1133. https://doi.org/10.1101/gad.300590.117.

15. Charizanis, K., Lee, K.Y., Batra, R., Goodwin, M., Zhang, C., Yuan, Y., Shiue, L., Cline, M., Scotti, M.M., Xia, G., et al. (2012). Muscleblind-like 2-mediated alternative splicing in the developing brain and dysregulation in myotonic dystrophy. Neuron *75*, 437–450. https://doi.org/10.1016/j.neuron.2012.05.029.

16. Wang, E.T., Treacy, D., Eichinger, K., Struck, A., Estabrook, J., Olafson, H., Wang, T.T., Bhatt, K., Westbrook, T., Sedehizadeh, S., et al. (2019). Transcriptome alterations in myotonic dystrophy skeletal muscle and heart. Hum. Mol. Genet. *28*, 1312–1321. https://doi.org/10.1093/hmg/ddy432.

17. Rau, F., Lainé, J., Ramanoudjame, L., Ferry, A., Arandel, L., Delalande, O., Jollet, A., Dingli, F., Lee, K.-Y., Peccate, C., et al. (2015). Abnormal splicing switch of DMD's penultimate exon compromises muscle fibre maintenance in myotonic dystrophy. Nat. Commun. *6*, 7205. https://doi.org/10.1038/ncomms8205.

18. Fugier, C., Klein, A.F., Hammer, C., Vassilopoulos, S., Ivarsson, Y., Toussaint, A., Tosch, V., Vignaud, A., Ferry, A., Messaddeq, N., et al. (2011). Misregulated alternative splicing of BIN1 is associated with T tubule alterations and muscle weakness in myotonic dystrophy. Nat. Med. *17*, 720–725. https://doi.org/10.1038/nm.2374.

19. Freyermuth, F., Rau, F., Kokunai, Y., Linke, T., Sellier, C., Nakamori, M., Kino, Y., Arandel, L., Jollet, A., Thibault, C., et al. (2016). Splicing misregulation of SCN5A contributes to cardiac-conduction delay and heart arrhythmia in myotonic dystrophy. Nat. Commun. *7*, 11067. https://doi.org/10.1038/ncomms11067.

20. Savkur, R.S., Philips, A.V., and Cooper, T.A. (2001). Aberrant regulation of insulin receptor alternative splicing is associated with insulin resistance in myotonic dystrophy. Nat. Genet. *29*, 40–47. https://doi.org/10.1038/ng704.

21. Charlet-B, N., Savkur, R.S., Singh, G., Philips, A.V., Grice, E.A., and Cooper, T.A. (2002). Loss of the muscle-specific chloride channel in type 1 myotonic dystrophy due to misregulated alternative splicing. Mol. Cell *10*, 45–53. https://doi.org/10.1016/S1097-2765(02)00572-5.

22. Mankodi, A., Takahashi, M.P., Jiang, H., Beck, C.L., Bowers, W.J., Moxley, R.T., Cannon, S.C., and Thornton, C.A. (2002). Expanded CUG repeats trigger aberrant splicing of ClC-1 chloride channel pre-mRNA and hyperexcitability of skeletal muscle in myotonic dystrophy. Mol. Cell *10*, 35–44. https://doi.org/10.1016/S1097-2765(02)00563-4.

23. Dirksen, R.T., Lueck, J.D., Swanson, M.S., Wheeler, T.M., Thornton, C.A., Swanson, M.S., Dirksen, R.T., and Thornton, C.A. (2007). Correction of ClC-1 splicing eliminates chloride channelopathy and myotonia in mouse models of myotonic dystrophy Find the latest version : correction of ClC-1 splicing eliminates chloride channelopathy and myotonia in mouse models of myotonic dystrophy. J. Clin. Invest. *117*, 3952–3957. https://doi.org/10.1172/JCI33355.3952.

24. Ashizawa, T., Gagnon, C., Groh, W.J., Gutmann, L., Johnson, N.E., Meola, G., Moxley, R., Pandya, S., Rogers, M.T., Simpson, E., et al. (2018). Consensus-based care recommendations for adults with myotonic dystrophy type 1. Neurol. Clin. Pract. *8*, 507–520. https://doi.org/10.1212/CPJ.0000000000000531.

25. Thomas, J.D., Oliveira, R., Sznajder, Ł.J., and Swanson, M.S. (2018). Myotonic dystrophy and developmental regulation of RNA processing. Compr. Physiol. *8*, 509–553. https://doi.org/10.1002/cphy.c170002.

26. Raaijmakers, R.H.L., Ripken, L., Ausems, C.R.M., Wansink, D.G., and Wansink, D.G. (2019). CRISPR/Cas applications in myotonic dystrophy : expanding opportunities. Int. J. Mol. Sci. *20*, 3689.

27. Pinto, B.S., Saxena, T., Oliveira, R., Méndez-Gómez, H.R., Cleary, J.D., Denes, L.T., McConnell, O., Arboleda, J., Xia, G., Swanson, M.S., and Wang, E.T. (2017). Impeding transcription of expanded microsatellite repeats by deactivated Cas9 impeding transcription of expanded microsatellite repeats by deactivated Cas9. Mol. Cell *68*, 479–490.e5. https://doi.org/10.1016/j.molcel.2017.09.033.

28. Batra, R., Nelles, D.A., Pirie, E., Blue, S.M., Marina, R.J., Wang, H., Chaim, I.A., Thomas, J.D., Zhang, N., Nguyen, V., et al. (2017). Elimination of toxic microsatellite repeat expansion article elimination of toxic microsatellite repeat expansion RNA by RNA-targeting Cas9. Cell *170*, 899–912.e10. https://doi.org/10.1016/j.cell.2017.07.010.

29. Thakore, P.I., D'Ippolito, A.M., Song, L., Safi, A., Shivakumar, N.K., Kabadi, A.M., Reddy, T.E., Crawford, G.E., and Gersbach, C.A. (2015). Highly specific epigenome editing by CRISPR-Cas9 repressors for silencing of distal regulatory elements. Nat. Methods *12*, 1143–1149. https://doi.org/10.1038/nmeth.3630.

30. Gilbert, L.A., Horlbeck, M.A., Adamson, B., Villalta, J.E., Chen, Y., Whitehead, E.H., Guimaraes, C., Panning, B., Ploegh, H.L., Bassik, M.C., et al. (2014). Genome-scale CRISPR-mediated control of gene repression and activation. Cell *159*, 647–661. https://doi.org/10.1016/j.cell.2014.09.029.

31. Pickar-Oliver, A., and Gersbach, C.A. (2019). The next generation of CRISPR–Cas technologies and applications. Nat. Rev. Mol. Cell Biol. *20*, 490–507. https://doi.org/10.1038/s41580-019-0131-5.

32. Dominguez, A.A., Lim, W.A., and Qi, L.S. (2016). Beyond editing: repurposing CRISPR-Cas9 for precision genome regulation and interrogation. Nat. Rev. Mol. Cell Biol. *17*, 5–15. https://doi.org/10.1038/nrm.2015.2.

33. Ying, Y., Yang, X., Zhao, K., Mao, J., Kuang, Y., Wang, Z., Sun, R., and Fei, J. (2015). The Krüppel-associated box repressor domain induces reversible and irreversible regulation of endogenous mouse genes by mediating different chromatin states. Nucleic Acids Res. *43*, 1549–1561. https://doi.org/10.1093/nar/gkv016.

34. Gilbert, L.A., Larson, M.H., Morsut, L., Liu, Z., Brar, G.A., Torres, S.E., Stern-Ginossar, N., Brandman, O., Whitehead, E.H., Doudna, J.A., et al. (2013). CRISPR-mediated modular RNA-guided regulation of transcription in eukaryotes. Cell *154*, 442–451. https://doi.org/10.1016/j.cell.2013.06.044.

35. Himeda, C.L., Jones, T.I., and Jones, P.L. (2016). CRISPR/dCas9-mediated transcriptional inhibition ameliorates the epigenetic dysregulation at D4Z4 and represses DUX4-fl in FSH muscular dystrophy. Mol. Ther. *24*, 527–535. https://doi.org/10.1038/mt.2015.200.

36. André, L.M., van Cruchten, R.T.P., Willemse, M., Bezstarosti, K., Demmers, J.A.A., van Agtmaal, E.L., Wansink, D.G., and Wieringa, B. (2019). Recovery in the myogenic program of congenital myotonic dystrophy myoblasts after excision of the expanded (CTG)n repeat. Int. J. Mol. Sci. *20*, 5685. https://doi.org/10.3390/ijms20225685.

37. Gudde, A.E., González-Barriga, A., van den Broek, W.J., Wieringa, B., and Wansink, D.G. (2016). A low absolute number of expanded transcripts is involved in myotonic dystrophy type 1 manifestation in muscle. Hum. Mol. Genet. *25*, 1648–1662. https://doi.org/10.1093/hmg/ddw042.

38. Furling, D., Lemieux, D., Taneja, K., and Puymirat, J. (2001). Decreased levels of myotonic dystrophy protein kinase (DMPK) and delayed differentiation in human myotonic dystrophy myoblasts. Neuromuscul. Disord. *11*, 728–735.

39. Arandel, L., Polay-Espinosa, M., Matloka, M., Bazinet, A., De Dea Diniz, D., Naouar, N., Rau, F., Jollet, A., Edom-Vovard, F., Mamchaoui, K., et al. (2017). Immortalized human myotonic dystrophy muscle cell lines to assess therapeutic compounds. Dis Model Mech, dmm. 027367. https://doi.org/10.1242/dmm.027367.

40. Jauvin, D., Chrétien, J., Pandey, S.K., Martineau, L., Revillod, L., Bassez, G., Lachon, A., MacLeod, A.R., Gourdon, G., Wheeler, T.M., et al. (2017). Targeting DMPK with antisense oligonucleotide improves muscle strength in myotonic dystrophy type 1 mice. Mol. Ther. Nucleic Acids *7*, 465–474. https://doi.org/10.1016/j.omtn.2017.05.007.

41. Klinck, R., Fourrier, A., Thibault, P., Toutant, J., Durand, M., Lapointe, E., Caillet-Boudin, M.L., Sergeant, N., Gourdon, G., Meola, G., et al. (2014). RBFOX1 cooperates with MBNL1 to control splicing in muscle, including events altered in myotonic dystrophy type 1. PLoS One *9*, 18–21. https://doi.org/10.1371/journal.pone.0107324.

42. Nakamori, M., Sobczak, K., Puwanant, A., Welle, S., Eichinger, K., Pandya, S., Dekdebrun, J., Heatwole, C.R., Mcdermott, M.P., Chen, T., et al. (2013). Splicing biomarkers of disease severity in myotonic dystrophy. Ann. Neurol. *74*, 862–872. https://doi.org/10.1002/ana.23992.

43. Trapnell, C., Williams, B.A., Pertea, G., Mortazavi, A., Kwan, G., Van Baren, M.J., Salzberg, S.L., Wold, B.J., and Pachter, L. (2010). Transcript assembly and quantification by RNA-Seq reveals unannotated transcripts and isoform switching during cell differentiation. Nat. Biotechnol. *28*, 511–515. https://doi.org/10.1038/nbt.1621.

44. Zhang, H., Wen, J., Bigot, A., Chen, J., Shang, R., Mouly, V., and Bi, P. (2020). Human Myotube Formation Is Determined by MyoD-Myomixer/Myomaker axis. Sci. Adv. https://doi.org/10.1126/sciadv.abc4062.

45. Spruston, N., and Johnston, D. (1992). Perforated patch-clamp analysis of the passive membrane properties of three classes of hippocampal neurons. J. Neurophysiol. *67*, 508–529. https://doi.org/10.1152/jn.1992.67.3.508.

46. François, V., Klein, A.F., Beley, C., Jollet, A., Lemercier, C., Garcia, L., and Furling, D. (2010). Selective silencing of mutated mRNAs in DM1 by using modified hU7-snRNAs. Nat. Struct. Mol. Biol. *18*, 85–87. https://doi.org/10.1038/nsmb.1958.

47. Klein, A.F., Varela, M.A., Arandel, L., Holland, A., Naouar, N., Arzumanov, A., Seoane, D., Revillod, L., Bassez, G., Ferry, A., et al. (2019). Peptide-conjugated oligonucleotides evoke long-lasting myotonic dystrophy correction in patient-derived cells and mice. J. Clin. Invest. *129*, 4739–4744. https://doi.org/10.1172/JCI128205.

48. Arandel, L., Matloka, M., Klein, A.F., Rau, F., Sureau, A., Ney, M., Cordier, A., Kondili, M., Polay-Espinoza, M., Naouar, N., et al. (2022). Reversal of RNA toxicity in myotonic dystrophy via a decoy RNA-binding protein with high affinity for expanded CUG repeats. Nat. Biomed. Eng. *6*, 207–220. https://doi.org/10.1038/s41551-021-00838-2.

49. Lo Scrudato, M., Poulard, K., Sourd, C., Tomé, S., Klein, A.F., Corre, G., Huguet, A., Furling, D., Gourdon, G., and Buj-Bello, A. (2019). Genome editing of expanded CTG repeats within the human DMPK gene reduces nuclear RNA foci in the muscle of DM1 mice. Mol. Ther. *27*, 1372–1388. https://doi.org/10.1016/j.ymthe.2019.05.021.

50. Benders, A.A., Timmermans, J.A., Oosterhof, A., Ter Laak, H.J., van Kuppevelt, T.H., Wevers, R.A., and Veerkamp, J.H. (1993). Deficiency of Na+/K+-ATPase and sarcoplasmic reticulum Ca2+-ATPase in skeletal muscle and cultured muscle cells of myotonic dystrophy patients. Biochem. J. *293*, 269–274. https://doi.org/10.1042/bj2930269.

51. Benders, A.A., Li, J., Lock, R.A., Bindels, R.J., Bonga, S.E., and Veerkamp, J.H. (1994). Copper toxicity in cultured human skeletal muscle cells: the involvement of Na+/K+-ATPase and the Na+/Ca2+-exchanger. Pflügers Archiv *428*, 461–467. https://doi.org/10.1007/BF00374566.

52. Behrens, M.I., Jalil, P., Serani, A., Vergara, F., and Alvarez, O. (1994). Possible role of apamin-sensitive K+ channels in myotonic dystrophy. Muscle Nerve *17*, 1264–1270.

53. Tajhya, R.B., Hu, X., Tanner, M.R., Huq, R., Kongchan, N., Neilson, J.R., Rodney, G.G., Horrigan, F.T., Timchenko, L.T., and Beeton, C. (2016). Functional KCa1.1 channels are crucial for regulating the proliferation, migration and differentiation of human primary skeletal myoblasts. Cell Death Dis. *7*, 1–12. https://doi.org/10.1038/cddis.2016.324.

54. Nurowska, E., Constanti, A., Dworakowska, B., Mouly, V., Furling, D., Lorenzon, P., Pietrangelo, T., Dołowy, K., and Ruzzier, F. (2009). Potassium currents in human myogenic cells from healthy and congenital myotonic dystrophy foetuses. Cell. Mol. Biol. Lett. *14*, 336–346. https://doi.org/10.2478/s11658-009-0006-4.

55. Franke, C., Hatt, H., Iaizzo, P.A., and Lehmann-Horn, F. (1990). Characteristics of Na+ channels and Cl- conductance in resealed muscle fibre segments from patients with myotonic dystrophy. J. Physiol. *425*, 391–405.

56. Waryah, C.B., Moses, C., Arooj, M., and Blancafort, P. (2018). Zinc fingers, TALEs, and CRISPR systems: a comparison of tools for epigenome editing. In Epigenome Editing (Methods in Molecular Biology), pp. 19–64.

57. Wegmann, S., DeVos, S.L., Zeitler, B., Marlen, K., Bennett, R.E., Perez-Rando, M., MacKenzie, D., Yu, Q., Commins, C., Bannon, R.N., et al. (2021). Persistent Repression of Tau in the Brain Using Engineered Zinc Finger Protein Transcription Factors. 2021. Sci. Adv. https://doi.org/10.1126/sciadv.abe1611.

58. Kim, D., Luk, K., Wolfe, S.A., and Kim, J.-S. (2019). Evaluating and enhancing target specificity of gene-editing nucleases and deaminases. Annu. Rev. Biochem. *88*, 191–220. https://doi.org/10.1146/annurev-biochem-013118-111730.

59. Leroux, A.E., Schulze, J.O., and Biondi, R.M. (2018). AGC kinases, mechanisms of regulation and innovative drug development. Semin. Cancer Biol. *48*, 1–17. https://doi.org/10.1016/j.semcancer.2017.05.011.

60. Jansen, G., Groenen, P.J., Bächner, D., Jap, P.H., Coerwinkel, M., Oerlemans, F., Van Den Broek, W., Gohlsch, B., Pette, D., Plomp, J.J., et al. (1996). Abnormal myotonic dystrophy protein kinase levels produce only mild myopathy in mice. Nat. Genet. *13*, 316–324. https://doi.org/10.1038/ng0796-316.

61. Reddy, S., Smith, D.B., Rich, M.M., Leferovich, J.M., Reilly, P., Davis, B.M., Tran, K., Rayburn, H., Bronson, R., Cros, D., et al. (1996). Mice lacking the myotonic dystrophy protein kinase develop a late onset progressive myopathy. Nat. Genet. *13*, 325–335. https://doi.org/10.1038/ng0796-325.

62. Berul, C.I., Maguire, C.T., Gehrmann, J., and Reddy, S. (2000). Progressive atrioventricular conduction block in a mouse myotonic dystrophy model. J. Intervent. Card Electrophysiol. *4*, 351–358. https://doi.org/10.1023/A:1009842114968.

63. Berul, C.I., Maguire, C.T., Aronovitz, M.J., Greenwood, J., Miller, C., Gehrmann, J., Housman, D., Mendelsohn, M.E., and Reddy, S. (1999). DMPK dosage alterations result in atrioventricular conduction abnormalities in a mouse myotonic dystrophy model. J. Clin. Invest. *103*, R1–R7. https://doi.org/10.1172/JCI5346.

64. Carrell, S.T., Carrell, E.M., Auerbach, D., Pandey, S.K., Bennett, C.F., Dirksen, R.T., and Thornton, C.A. (2016). Dmpk gene deletion or antisense knockdown does not compromise cardiac or skeletal muscle function in mice. Hum. Mol. Genet. *25*, 4328–4338. https://doi.org/10.1093/hmg/ddw266.

65. Pandey, S.K., Wheeler, T.M., Justice, S.L., Kim, A., Younis, H.S., Gattis, D., Jauvin, D., Puymirat, J., Swayze, E.E., Freier, S.M., et al. (2015). Identification and characterization of modified antisense oligonucleotides targeting DMPK in mice and nonhuman primates for the treatment of myotonic dystrophy type 1. J. Pharmacol. Exp. Therapeut. *355*, 329–340.

66. Thornton, C.A., Wang, E., and Carrell, E.M. (2017). Myotonic dystrophy: approach to therapy. Curr. Opin. Genet. Dev. *44*, 135–140. https://doi.org/10.1016/j.gde.2017.03.007.

67. Angelbello, A.J., Rzuczek, S.G., Mckee, K.K., Chen, J.L., Olafson, H., Cameron, M.D., Moss, W.N., Wang, E.T., and Disney, M.D. (2019). Precise small-molecule cleavage of an r (CUG) repeat expansion in a myotonic dystrophy mouse model. Proc. Natl. Acad. Sci. USA *116*, 7799–7804. https://doi.org/10.1073/pnas.1901484116.

68. Tomé, S., and Gourdon, G. (2020). DM1 phenotype variability and triplet repeat instability: challenges in the development of new therapies. Int. J. Mol. Sci. *21*, 457. https://doi.org/10.3390/ijms21020457.

69. Zu, T., Gibbens, B., Doty, N.S., Gomes-Pereira, M., Huguet, A., Stone, M.D., Margolis, J., Peterson, M., Markowski, T.W., Ingram, M.A.C., et al. (2011). Non-ATG-initiated translation directed by microsatellite expansions. Proc. Natl. Acad. Sci. USA *108*, 260–265. https://doi.org/10.1073/pnas.1013343108.

70. Nguyen, L., Cleary, J.D., and Ranum, L.P.W. (2019). Repeat-associated non-ATG translation: molecular mechanisms and contribution to neurological disease. Annu. Rev. Neurosci. *42*, 227–247. https://doi.org/10.1146/annurev-neuro-070918-050405.

71. Li, C., and Samulski, R.J. (2020). Engineering adeno-associated virus vectors for gene therapy. Nat. Rev. Genet. *21*, 255–272. https://doi.org/10.1038/s41576-019-0205-4.

72. Colella, P., Ronzitti, G., and Mingozzi, F. (2018). Emerging issues in AAV-mediated in vivo gene therapy. Mol. Ther. Methods Clin. Dev. *8*, 87–104. https://doi.org/10.1016/j.omtm.2017.11.007.

73. Thorley, M., Duguez, S., Mazza, E.M.C., Valsoni, S., Bigot, A., Mamchaoui, K., Harmon, B., Voit, T., Mouly, V., Duddy, W., et al. (2016). Skeletal muscle characteristics are preserved in hTERT/cdk4 human myogenic cell lines. Skeletal Muscle *6*, 1–12. https://doi.org/10.1186/s13395-016-0115-5.

74. Mamchaoui, K., Trollet, C., Bigot, A., Negroni, E., Chaouch, S., Wolff, A., Kandalla, P.K., Marie, S., Di Santo, J., St Guily, J.L., et al. (2011). Immortalized pathological human myoblasts : towards a universal tool for the study of neuromuscular disorders. Skeletal Muscle *1*, 34.

75. Bigot, A., Klein, A.F., Gasnier, E., Jacquemin, V., Ravassard, P., Butler-Browne, G., Mouly, V., and Furling, D. (2009). Large CTG repeats trigger p16-dependent premature senescence in myotonic dystrophy type 1 muscle precursor cells. Am. J. Pathol. *174*, 1435–1442. https://doi.org/10.2353/ajpath.2009.080560.

76. Radzisheuskaya, A., Shlyueva, D., Müller, I., and Helin, K. (2016). Optimizing sgRNA position markedly improves the efficiency of CRISPR/dCas9-mediated transcriptional repression. Nucleic Acids Res. *44*, 1–13. https://doi.org/10.1093/nar/gkw583.

77. Horlbeck, M.A., Gilbert, L.A., Villalta, J.E., Adamson, B., Pak, R.A., Chen, Y., Fields, A.P., Park, C.Y., Corn, J.E., Kampmann, M., and Weissman, J.S. (2016). Compact and highly active next-generation libraries for CRISPR-mediated gene repression and activation. Elife *5*, 1197600–1197620. https://doi.org/10.7554/eLife.19760.

78. Mandegar, M.A., Huebsch, N., Frolov, E.B., Shin, E., Truong, A., Olvera, M.P., Chan, A.H., Miyaoka, Y., Holmes, K., Spencer, C.I., et al. (2016). CRISPR interference efficiently induces specific and reversible gene silencing in human iPSCs. Cell Stem Cell *18*, 541–553. https://doi.org/10.1016/j.stem.2016.01.022.

79. Heigwer, F., Kerr, G., and Boutros, M. (2014). E-CRISP: fast CRISPR target site identification. Nat. Methods *11*, 122–123. https://doi.org/10.1038/nmeth.2812.

80. Liu, H., Wei, Z., Dominguez, A., Li, Y., Wang, X., and Qi, L.S. (2015). CRISPR-ERA: a comprehensive design tool for CRISPR-mediated gene editing, repression and activation. Bioinformatics *31*, 3676–3678. https://doi.org/10.1093/bioinformatics/btv423.

81. Moreno-Mateos, M.A., Vejnar, C.E., Beaudoin, J.D., Fernandez, J.P., Mis, E.K., Khokha, M.K., and Giraldez, A.J. (2015). CRISPRscan: designing highly efficient sgRNAs for CRISPR-Cas9 targeting in vivo. Nat. Methods *12*, 982–988. https://doi.org/10.1038/nmeth.3543.

82. Labun, K., Montague, T.G., Gagnon, J.A., Thyme, S.B., and Valen, E. (2016). CHOPCHOP v2: a web tool for the next generation of CRISPR genome engineering. Nucleic Acids Res. *44*, W272–W276. https://doi.org/10.1093/nar/gkw398.

83. Stemmer, M., Thumberger, T., Del Sol Keyer, M., Wittbrodt, J., and Mateo, J.L. (2015). CCTop: an intuitive, flexible and reliable CRISPR/Cas9 target prediction tool. PLoS One *10*, 1–11. https://doi.org/10.1371/journal.pone.0124633.

84. Doench, J.G., Fusi, N., Sullender, M., Hegde, M., Vaimberg, E.W., Donovan, K.F., Smith, I., Tothova, Z., Wilen, C., Orchard, R., et al. (2016). Optimized sgRNA design to maximize activity and minimize off-target effects of CRISPR-Cas9. Nat. Biotechnol. *34*, 184–191. https://doi.org/10.1038/nbt.3437.

85. Sanson, K.R., Hanna, R.E., Hegde, M., Donovan, K.F., Strand, C., Sullender, M.E., Vaimberg, E.W., Goodale, A., Root, D.E., Piccioni, F., and Doench, J.G. (2018). Optimized libraries for CRISPR-Cas9 genetic screens with multiple modalities. Nat. Commun. *9*, 5416–5515. https://doi.org/10.1038/s41467-018-07901-8.

86. Sanjana, N.E., Shalem, O., and Zhang, F. (2014). Improved vectors and genome-wide libraries for CRISPR screening. Nat. Methods *11*, 783–784. https://doi.org/10.1038/nmeth.3047.

87. Emi, N., Friedmann, T., and Yee, J.K. (1991). Pseudotype formation of murine leukemia virus with the G protein of vesicular stomatitis virus. J. Virol. *65*, 1202–1207. https://doi.org/10.1128/jvi.65.3.1202-1207.1991.

88. Klein, A.F., Arandel, L., Marie, J., and Furling, D. (2020). FISH protocol for myotonic dystrophy type 1 cells. Methods Mol. Biol. *2056*, 203–215. https://doi.org/10.1007/978-1-4939-9784-8_13.

89. Otsu, N. (1979). A threshold selection method from gray-level histograms. IEEE Trans. Syst. Man Cybern. *9*, 62–66.

90. Chujo, T., Yamazaki, T., Kawaguchi, T., Kurosaka, S., Takumi, T., Nakagawa, S., and Hirose, T. (2017). Unusual semi-extractability as a hallmark of nuclear body-associated architectural noncoding RNAs. EMBO J. *36*, 1447–1462. https://doi.org/10.15252/embj.201695848.

91. Nutter, C.A., Bubenik, J.L., Oliveira, R., Ivankovic, F., Sznajder, Ł.J., Kidd, B.M., Pinto, B.S., Otero, B.A., Carter, H.A., Vitriol, E.A., et al. (2019). Cell-type-specific dysregulation of RNA alternative splicing in short tandem repeat mouse knockin models of myotonic dystrophy. Genes Dev. *33*, 1635–1640. https://doi.org/10.1101/gad.328963.119.

92. Poitras, E., and Houde, A. (2002). La PCR en temps réel: principes et applications. Reviews in Biology and Biotechnology *2*, 2–11.

93. Stern-Straeter, J., Bonaterra, G.A., Hörmann, K., Kinscherf, R., and Goessler, U.R. (2009). Identification of valid reference genes during the differentiation of human myoblasts. BMC Mol. Biol. *10*, 1–9. https://doi.org/10.1186/1471-2199-10-66.

94. Hubaux, R., Vandermeers, F., Cosse, J.P., Crisanti, C., Kapoor, V., Albelda, S.M., Mascaux, C., Delvenne, P., Hubert, P., and Willems, L. (2015). Valproic acid improves second-line regimen of small cell lung carcinoma in preclinical models. ERJ Open Res *1*, 00028–02015.

95. Eriksson, M. (2004). Real-time RT-PCR for CTG repeat-containing genes. Methods Mol. Biol. *277*, 77–84. https://doi.org/10.1385/1-59259-804-8:077.

96. Martin, M. (2011). Cutadapt removes adapter sequences from high-throughput sequencing reads. EMBnet *17*, 10–12.

97. Dobin, A., Davis, C.A., Schlesinger, F., Drenkow, J., Zaleski, C., Jha, S., Batut, P., Chaisson, M., and Gingeras, T.R. (2013). STAR: ultrafast universal RNA-seq aligner. Bioinformatics *29*, 15–21. https://doi.org/10.1093/bioinformatics/bts635.

98. Anders, S., Pyl, P.T., and Huber, W. (2015). HTSeq-A Python framework to work with high-throughput sequencing data. Bioinformatics *31*, 166–169. https://doi.org/10.1093/bioinformatics/btu638.

99. Shen, S., Park, J.W., Lu, Z.X., Lin, L., Henry, M.D., Wu, Y.N., Zhou, Q., and Xing, Y. (2014). rMATS: robust and flexible detection of differential alternative splicing from replicate RNA-Seq data. Proc. Natl. Acad. Sci. USA *111*, E5593–E5601. https://doi.org/10.1073/pnas.1419161111.

100. Love, M.I., Huber, W., and Anders, S. (2014). Moderated estimation of fold change and dispersion for RNA-seq data with DESeq2. Genome Biol. *15*, 550–621. https://doi.org/10.1186/s13059-014-0550-8.

101. Babicki, S., Arndt, D., Marcu, A., Liang, Y., Grant, J.R., Maciejewski, A., and Wishart, D.S. (2016). Heatmapper: web-enabled heat mapping for all. Nucleic Acids Res. *44*, W147–W153. https://doi.org/10.1093/NAR/GKW419.

102. Liao, Y., Wang, J., Jaehnig, E.J., Shi, Z., and Zhang, B. (2019). WebGestalt 2019: gene set analysis toolkit with revamped UIs and APIs. Nucleic Acids Res. *47*, W199–W205. https://doi.org/10.1093/nar/gkz401.

103. Aken, B.L., Ayling, S., Barrell, D., Clarke, L., Curwen, V., Fairley, S., Fernandez Banet, J., Billis, K., García Girón, C., Hourlier, T., et al. (2016). The Ensembl gene annotation system. Database *2016*, 1–19. https://doi.org/10.1093/database/baw093.

104. Liao, Y., Smyth, G.K., and Shi, W. (2014). FeatureCounts: an efficient general purpose program for assigning sequence reads to genomic features. Bioinformatics *30*, 923–930. https://doi.org/10.1093/bioinformatics/btt656.

105. Noble, W.S. (2009). How does multiple testing correction work? Nat. Biotechnol. *27*, 1135–1137. https://doi.org/10.1038/nbt1209-1135.